STRUCTURES OF ANGLED AERATED-LIQUID JETS IN MACH 1.94 SUPERSONIC CROSSFLOW

THESIS

Dion R. Dixon, 1st Lieutenant, USAF

AFIT/GAE/ENY/05-M07

DEPARTMENT OF THE AIR FORCE
AIR UNIVERSITY

AIR FORCE INSTITUTE OF TECHNOLOGY

Wright-Patterson Air Force Base, Ohio

The views expressed in this thesis are those of the author and do not reflect the official policy or position of the United State Air Force, Department of Defense, or the United States Government.

AFIT/GAE/ENY/05-M07

STRUCTURES OF ANGLED AERATED-LIQUID JETS IN MACH 1.94 SUPERSONIC CROSSFLOW

THESIS

Presented to the Faculty

Department of Systems and Engineering Management

Graduate School of Engineering and Management

Air Force Institute of Technology

Air University

Air Education and Training Command

In Partial Fulfillment of the Requirements for the

Degree of Master of Science in Aeronautical Engineering

Dion R. Dixon, BS

1st Lieutenant, USAF

March 2005

AFIT/GAE/ENY/05-M07

STRUCTURES OF ANGLED AERATED-LIQUID JETS IN MACH 1.94 SUPERSONIC CROSSFLOW

Dion R. Dixon, BS
1st Lieutenant, USAF

Approved:

Ralph A. Anthenien (Chairman)	date
Paul I. King (Member)	date
Mark R. Gruber (Member)	date

Abstract

The structures of aerated-liquid jets injected into a supersonic crossflow have been studied experimentally. Aerated-liquid injectors with diameters of 0.020" (0.5 mm), 0.040" (1.0 mm) and 0.060" (1.5 mm) were flush mounted on the bottom plate of a supersonic wind tunnel to provide normal and angled injection. Freestream Mach number and temperature were held constant at 1.94 and 500 °F (960 °R), respectively. Water at room temperature was used as the liquid injectant and nitrogen gas used as the aerating gas. Wide ranges of test conditions for injection angle (θ), injector orifice diameter (d_0), jet-to-air momentum flux ratios (q_0), and gas-to-liquid ratios (GLR), were studied. Injection angles were varied from 45° downstream to 90° (normal to freestream). Jet-to-air momentum flux was varied from 1% to 15% of the freestream and gas-to-liquid ratios from 0% (pure-liquid injection) to 10%. Shadowgraph and laser sheet illumination techniques were used for spray visualization while a phase Doppler particle analyzer (PDPA) was utilized to quantitatively measure droplet and spray plume properties. The data from all three methods were used to develop correlations for the droplet and spray plume properties for aerated-liquid jets using a linear fit of the base-10 logarithm coefficients. Correlations relating penetration height and spray plume width of the injected spray to the above listed parameters, as well as the normalized axial distance downstream of the injector, x/d_0, were formulated based on all three measurement techniques. Results indicate that a reasonable prediction of penetration height, spray plume cross sectional area, and local equivalence ratio can be obtained from PDPA data, while other visualization techniques tend to under-predict such quantities.

To my Mom and Dad, without whose persistence and love I never could have achieved my goals, and whose insistence on the constant pursuit of knowledge has led me here today and will continue to drive me toward horizons beyond...

Acknowledgments

First and foremost, I would like to thank God, to whom I owe all I am and have. My parents, who have always been my biggest supporters, are also owed a great deal of thanks. I would like to express my sincere appreciation to Colonel Michael A. Heil and Mr. Parker Buckley, for allowing me to take the time each day during these past couple years to pursue my degree. I would also like to thank my coworkers in the Propulsion Directorate, for their guidance, advice, and vast wealth of knowledge. I would especially like to thank Dr. Kuo-Cheng (Steven) Lin, whose mentoring was invaluable in this effort. My appreciation also goes to Dr. Richard Anthony, who never seemed to tire of my constant Matlab questions throughout this whole process. Finally, I would like to thank my advisors, Dr. Ralph A. Anthenien and Dr. Mark R. Gruber, who were instrumental in helping to turn raw data and numbers into the written work you see before you.

Dion R. Dixon

Table of Contents

List of Figures

measurements. The test conditions for each of these plots are as follows: a) θ=45°, d_0=0.020". q_0=3, GLR=7%, b) θ=45°, d_0=0.020". q_0=7, GLR=5%, c) θ=60°, d_0=0.020". q_0=5, GLR=5%, d) θ=60°, d_0=0.020". q_0=6, GLR=2%, e) θ=75°, d_0=0.020". q_0=5, GLR=3%, f) θ=75°, d_0=0.020". q_0=10, GLR=0%, g) θ=90°, d_0=0.020". q_0=3, GLR=0%, h) θ=90°, d_0=0.020". q_0=3, GLR=8%. (Plumes are shown half-width.) *Denotes PDPA measurements taken by Lin et al.[12] included for completeness.

List of Tables

List of Symbols

α	= thermal diffusivity
B	= mass transfer number
d	= droplet diameter
d_0	= injector orifice diameter
GLR	= aerating gas-to-liquid mass ratio (in percentage)
h	= spray penetration height
L	= nozzle passage length
M	= freestream Mach number
Q	= volumetric flow rate
Q_{inj}	= measured volumetric liquid flow rate from flow meter
Q_m	= integrated volumetric liquid flow rate from PDPA volume flux measurement
q_0	= jet-to-freestream momentum flux ratio at GLR=0, $\rho_0 w_0^2/\rho_\infty u_\infty^2$
ρ	= density
SMD	= Sauter mean diameter, $\sum d_i^3/\sum d_i^2$, i for all droplets
t_b	= burning time
T	= static temperature
T_0	= total temperature
u	= velocity component in the x-direction
v	= velocity component in the y direction
w	= velocity component in the z-direction
w_s	= spray width
x	= axial position downstream of the injector exit centerline
y	= vertical distance from the wind tunnel bottom floor (in the direction of liquid injection)
z	= distance in the transverse direction
θ	= injection angle relative to the freestream direction

STRUCTURES OF ANGLED AERATED-LIQUID JETS IN MACH 1.94 SUPERSONIC CROSSFLOW

INTRODUCTION

In the pursuit of aviation advances, three main goals have dictated much of the research to date: higher, faster, and farther. Atmospheric flight has consistently striven to reach far above the ground, to fly at the utmost speed, and to span the vast distances that separate the peoples of the earth. Particularly in the pursuit of speed, hypersonic airbreathing propulsion has been a key focus in the last several decades.

Hypersonic atmospheric flight is nothing new; the USAF X-15 regularly flew greater than Mach 5 during its ten year testing phase. However, until recently, hypersonic velocities in powered atmospheric flight have only been obtainable through the use of rocket propulsion. This required the vehicles to carry large amounts of heavy oxidizer on board, limiting payload and/or crew capacity. By developing an airbreathing hypersonic propulsion system, more internal space and weight-carrying capacity is available for accomplishing the mission.

To achieve such great speed, a method of capturing and compressing the incoming air is needed that will not generate excessive drag. Thus, the rotating turbomachinery of turbojet (and later turbofan) engines could not be used to travel faster than high supersonic speeds, perhaps as high as Mach 2.5. The ramjet engine was developed to achieve higher velocities without the drag penalty of the turbomachinery. The ramjet uses its own high momentum to compress air from the atmosphere, combusting it with the fuel carried on board. In a ramjet engine, the incoming air is compressed and slowed to subsonic speeds in order to mix and combust with the fuel. Problems arise in speeds greater than about Mach 5, where temperature increases due to deceleration and compression of the incoming air heat the engine and/or vehicle above operable limits.

The concept of a supersonic combustion ramjet (scramjet), a type of ramjet in which the incoming air is slowed to a low supersonic speed, rather than subsonic, was hypothesized in the early 1900's, shortly after the advent of heavier-than-air flight, and explored in the years following World War II. While the concept is fairly simple and straightforward, implementation has hardly been considered easy by the aeronautical community. Rather, many key technical hurdles have been discovered and overcome in the pursuit of hypersonic atmospheric flight.

Of the many technological hurdles facing airbreathing hypersonic flight, a key stumbling block that still requires extensive research is the problem of igniting and maintaining the combustion process in the scramjet engine. With current experimental engines measuring on the order of one meter in length, and internal flow velocities on the order of one kilometer per second, residence times of captured air approach one millisecond. The ability to mix and ignite a combustible mixture in such an environment has been likened to "lighting a match in a hurricane."

Of pivotal importance to achieving ignition and sustained combustion of a liquid fuel/air mixture is the ability to atomize the fuel spray as it is injected into the freestream air. Atomization processes reduce the droplet size of the injected fuel, promoting evaporation of the fuel into a gaseous phase, which is required for combustion. Many different techniques have been utilized in liquid spray systems to accomplish atomization, though because of weight and size limitations, the aeration (a.k.a. barbotage or effervescent) technique has been chosen for scramjet considerations.

The aeration technique involves a process by which small, highly-pressurized bubbles of a gas are injected into a liquid flow. These bubbles have the effect of 1) breaking up the liquid column prior to injection into the freestream air, and 2) adding momentum to the liquid spray,

thereby increasing its penetration height into a crossflow of air. In typical scramjet fueling configurations, the liquid fuel would most likely be kerosene or a derivative, and gaseous hydrogen the aerating gas. In this configuration, the choice of hydrogen as the aerating gas has the added benefit of promoting the ignition process because of the volatile nature of hydrogen gas, as well as introducing OH^- radicals into the reaction, further promoting burning of the larger hydrocarbon chains.

In order to fully capitalize on the potential benefits of such a fueling scheme, the fundamental physics underlying the technique must be understood. Studies have been conducted to determine the characteristics of aerated-liquid jets, from quiescent to subsonic to supersonic environments. While studies conducted in quiescent environments have been helpful in understanding the basic phenomena involved in the liquid column breakup process as initiated by the aeration method, such studies are not representative of the types of environments encountered in a scramjet combustor. By the nature of its design, the freestream flow is supersonic through a scramjet combustor, thereby requiring the study of aerated-liquid sprays in a supersonic environment. However, previous studies conducted in subsonic environments still yield useful data, due to the presence of a localized subsonic region behind the flame-induced shock front during the combustion process.

Penetration height is a key factor in determining the effectiveness of a fuel injector in a scramjet combustor. Because the incoming freestream air has a large amount of momentum itself, any fuel spray injected into it must have sufficient momentum to penetrate the boundary layer and provide sufficient fueling to the core flow. Studies conducted with pure-liquid jets in a supersonic crossflow have shown that they lack sufficient momentum to penetrate deeply into the core flow, particularly when droplet sizes are small, starving the core of fuel and leading to

inefficient combustion. Aerating the liquid jet introduces an effective net gain in momentum, as well as aiding in the atomization process, and therefore introduces greater amounts of small fuel droplets into the core flow.

It has been found through previous study that the angle of injection, the size and shape of the injection orifice, the ratio of jet to freestream air momentum flux, and the amount of aeration added to the spray all contribute in varying degrees to the amount of penetration height gained. However, these factors have not been thoroughly investigated, especially since the introduction of more highly detailed data collection techniques, such as phase Doppler particle anemometry. As such, it is necessary to investigate these contributing factors and develop a more thorough knowledge base of their effects on aerated-liquid sprays. To aid in the future development and design of aerated-liquid injectors, correlations between these factors and spray penetration height are needed.

The objective of this study is to further characterize the spray plume emanating from an aerated-liquid injector and to develop more accurate correlations between penetration height of the spray plume, and the following four parameters: injection angle, injector orifice diameter, jet-to-freestream momentum flux ratio, and gas-to-liquid ratio. These correlations will prove useful in the future design of scramjet fueling mechanisms and should result in more effective ignition and more efficient combustion in the scramjet engine. The following chapters provide a review of the work done previously in this field, a description of the test setup and methods of the present study, an analysis of the data collected, and conclusions arrived at from the data.

LITERATURE REVIEW

In order to combust, a fuel/air mixture must be in a gaseous phase. As such, liquid fuels must first be atomized to create small droplets which will evaporate quickly, and thus react with the present oxidizer. Kanury[1] gives a relationship of the amount of time it takes for a droplet of fuel to burn to physical properties of the fuel and air (see Eq. 1 below).

$$t_b \equiv \frac{d_0^2}{\frac{8\rho_g \alpha_g}{\rho_l}\ln(B+1)} \qquad \textbf{Eq. 1}$$

Because burning time of a droplet is directly related to the square of the droplet diameter, droplet size must be kept to a minimum in order to achieve a fast burning time. It is evident that a fast burning time is conducive to quick initiation of a flame front, which is necessary in the short residence times encountered in scramjet combustors.

Numerous methods have been employed to atomize liquid sprays in a variety of applications, ranging from agriculture to household products to the aerospace industry. The most frequently employed atomization methods are pressure atomization, pneumatic atomization, and impinging jets. Pressure atomizers work by simply injecting the liquid spray through an orifice at high velocity, typically with swirl, into relatively quiescent air. This process forms an unstable conical film of liquid, which in turn leads to the generation of holes and waves in the film, initiating the break up of the film into drops. These types of atomizers are commonly found in gas automotive applications.

Pneumatic atomization uses a high velocity stream of air (or other gas) flowing by a relatively low velocity jet of liquid. The resulting surface drag between the air and liquid flows produces distortions in the liquid jet and promotes the break up of the jet into fine droplets. This type of atomization can be found in everyday use in items such as a paint spray gun or gas

turbine engines. With the impinging jets technique, two jets of liquid are made to collide head-on into each other, forming a sheet at the stagnation point with an unstable nature. Alternatively, a single jet may be made to collide with a solid wall, with the same results. Impinging jet atomizers have been widely used in liquid-fueled rocket motors in the past, though modern rocket motors now use pressure atomizers.[1]

Of these three, the pneumatic atomizer produces the smallest average droplet sizes. Gretzinger et al.[2] were the first to thoroughly characterize the sprays of pneumatic nozzles and arrive at correlations between droplet size and nozzle parameters. Not only was it confirmed that pneumatic atomization methods more efficiently produced smaller droplets than mechanical means, but it was also observed that the thinner the liquid jet is squeezed by the co-flowing air, the smaller the droplets produced.

It is unclear as to who may have first theorized the idea of aerating the liquid stream or when, but Lefebvre et al.[3] were among the first to attempt a detailed characterization of this new and innovative method of achieving atomization. Whereas in pneumatic atomization, a relatively high velocity air stream is introduced to an already-formed liquid jet, the aerating method instead introduces bubbles of relatively low velocity gas into the liquid prior to the liquid spray being ejected from the nozzle orifice. This method should not be confused with supercritical injection, which relies on the flash vaporizing of dissolved gas in the liquid. It has been found that the bubble growth rate from dissolved gasses in the liquid is relatively slow and usually requires the use of an expansion chamber in the nozzle (thus creating the need for excess volume). Because of this limitation, both the slow bubble growth (which relates directly to slow atomization processes) and the need for additional volume where volume surplus is extremely limited, supercritical injection methods are not well suited to use in scramjet applications.

Lefebvre et al.[3] experimented by injecting water from an aerated-liquid injector into air at normal atmospheric pressure and temperature. Measurements were taken using a Malvern particle size analyzer, which is based on the Fraunhofer diffraction theory. It was found that the aerated-liquid injector produced better atomization characteristics at lower injection pressures than similarly sized pressure swirl or air-assist atomizers. It was also observed that the Sauter Mean Diameter (SMD) of droplets was almost entirely below 100 μm at gas-to-liquid mass ratios (GLR) of 2% or greater (by mass), and that increasing the amount of aerating gas would continue to reduce droplet size. Thus, a relatively small amount of aerating gas can drastically reduce the mean droplet size in the spray, especially when compared with more traditional atomization techniques. Lefebvre et al. concluded that the aerated-liquid injector system offered the following advantages over pressure swirl or air-assist atomizers: relatively large holes and passages throughout the nozzle which greatly reduce the problems of plugging and coking, alleviation of soot formation and exhaust smoke due to the presence of air bubbles in the spray, and ease of maintenance and low cost because of the simplicity of the design.

To better understand the fundamental physics involved in aerated-liquid sprays, Lin et al.[4] manufactured a clear aerated-liquid injector nozzle to study the two-phase internal flow and the near-field structures of the corresponding spray. From their observations, it was realized that the overall appearance (spray plume height, width, cross-sectional area) of the aerated-liquid spray is strongly related to the structure of the two-phase flow inside the discharge passage. They found that, as the amount of aerating gas is increased, the two-phase mixture has an increasingly co-annular flow structure where the gas forms a core inside a hollow column of liquid. The more aerating gas injected, the thinner the column walls of the liquid tube. As the near-field spray was observed, it was found that the thinner the column walls of the liquid tube,

the smaller the droplets produced when the liquid column shattered. This observation concurred well with the observations made by Lefebvre et al.[3]

In regards to fueling a scramjet combustor, two schools of thought have arisen, the use of fuel injecting pylons that project into the flow, or the use of flush-mounted wall injectors. Both types of fuel injection schemes have seen successful implementation, but the trend seems to be toward flush-mounted injectors, in part because of the success of aerated-liquid injection. Pylon injectors have the disadvantage of obstructing flow in the combustor section, thereby creating drag, which in turn not only causes a thrust penalty in the engine, but also creates localized heating on the pylon itself, necessitating a cooling system in each pylon. Flush-mounted injectors present no obstruction to the flow through the combustor. Pylon injectors do have an advantage in that they are capable of injecting fuel at any vertical station in the combustor, including directly into the core flow. Combined with the pylon's ability to act as a flameholder device due to the recirculating flow behind it, the design was a good first candidate for piloting and fueling the combustion section of a scramjet engine.

Sabel'nikov et al.[5] performed a study in which they compared a tube-micropylon injecting aerated-liquid kerosene at 45° downstream with a fin-pylon injecting parallel to the freestream. Their measurements were based on combustion efficiency derived from axial static pressure distributions and calculated pressure-area integrals. Their findings suggested that the angled tube-micropylon injector had better mixing characteristics than the fin-pylon, which may have been attributed to the fin-pylon shielding the high momentum freestream air from fully interacting with the injected stream. A part of their study also focused on the use of hydrogen gas and air as different aerating mediums and found that hydrogen produced slightly better combustion efficiencies. This is to be expected because of hydrogen's volatile nature and the

extreme close proximity of the hydrogen molecules to the liquid fuel droplets, as well as the addition of OH^- radicals to the fuel/air mixture.

Mathur et al.[6] achieved successful sustained combustion in a direct-connect scramjet engine fueled by warm liquid JP-7. Liquid JP-7 is the fuel of choice for the United States Air Force because of its relatively high energy density, existing logistics (from previous use with the SR-71 airframe), and ease of handling. While similar in nature to kerosene, JP-7 was specially formulated for high thermal stability and consists of long hydrocarbon chains, which must be cracked, or broken into smaller chains. Cracking occurs at high temperatures, a feature of JP-7 that, along with its endothermic nature, has made JP-7 in particular a good candidate as not only a fuel, but also as a heat sink for vehicle and engine cooling. In a closed-loop system, JP-7 could be run through cooling channels in the vehicle and engine skin, absorbing heat from aerodynamic friction drag on the body and the combustion process inside the engine, which would in turn crack the fuel and prepare it for injection into the combustion chamber. Experiments conducted by Mathur et al.[6] involved injecting liquid JP-7 from flush-mounted orifices on the top and bottom walls of a two-dimensional scramjet combustor simulating flight Mach numbers between 4 and 8. Their experiments were repeatable and sustainable, producing net positive thrust as measured by a load cell mounted to the thrust stand and calculated through the use of calorimetry of the combustor exhaust gases. Oxygen was introduced as an aerating gas in the bottom mounted injectors and it was observed that combustion efficiency was slightly greater for these injectors than for the pure-liquid injectors on the top wall.

Figure 1 shows the typical breakup process encountered in aerated-liquid injection into a supersonic crossflow. This type of breakup process has been observed consistently in experiments conducted in the supersonic regime. Of note is the co-annular flow of gas and

liquid at the injector orifice exit, which aids in the aerodynamic shearing of the liquid wall by compressing the liquid column wall into a thinner sheet. The liquid column is then further broken apart into ligaments and droplets by the supersonic crossflow.

Concurrently and following the successful use of aerated-liquid fuel sprays in a scramjet engine, Lin et al.[7-12] studied aerated-liquid injection in a variety of environments and over a wide range of parameters to better understand the fundamental flow characteristics. Many of these studies were conducted in supersonic crossflows, an environment more typical of a scramjet combustor. In a study by Lin et al.[7], water, alcohol, and a 33% alcohol/water solution were injected into Mach 1.85 supersonic crossflow through an aerated-liquid injector. Spray visualization was accomplished through the use of shadowgraphy and laser sheet illumination. During this effort, the effect of jet-to-air momentum flux ratio on penetration height of the spray was studied. Virtually no difference was noted in the penetration heights of the different injectant liquids, despite the differences in their physical properties, which suggests that liquids of varying viscosity, surface tension, and density may be used and still be within a reasonable range of predictable behavior. The following correlation was determined from measurements of spray plume height in the various imagery[7]:

$$\frac{h}{d_0} = 9.3 * q_0^{0.41} \qquad \textbf{Eq. 2}$$

Lin et al.[8] examined the effect of various injection angles on penetration height of the aerated-liquid spray. Again, water, alcohol, and an alcohol/water mixture were used as the test injectants and injection angles of 90° (normal to the freestream flow), 60°, and 30° downstream were tested. Shadowgraphy provided spray visualization while laser Doppler velocimetry was

used to measure the freestream velocity profile at the injection location. From the data, the following correlation was hypothesized, taking into account injection angle:

$$\frac{h}{d_0} = 8.4 * q_0^{0.44} * \sin(\theta) \qquad \textbf{Eq. 3}$$

From inspection, it can be seen that this correlation does not provide useful predictions for parallel injection (θ=0). In later work, Lin et al.[9] injected water and alcohol from an aerated-liquid injector into a subsonic crossflow. While the purpose of a scramjet engine is to avoid the losses encountered in a traditional ramjet engine when decelerating the flow to subsonic speeds, there are instances, particularly at low flight Mach numbers (M<6), where a scramjet combustor may experience localized pockets of subsonic flow. An example would be the region behind the flame-induced shock train, exactly the portion of the engine which would see fuel injection. From measurements of the spray boundary taken up to 90 diameters downstream of the injector centerline, the following correlation was derived to relate penetration height of the spray to the momentum flux and downstream axial distance for normal injection:

$$\frac{h}{d_0} = 2.42 * q_0^{0.48} * \left(\frac{w}{d_0}\right)^{0.24} \qquad \textbf{Eq. 4}$$

For the studies conducted by Lin et al.[10], pure- and aerated-liquid jets in subsonic (up to Mach 0.4) and supersonic (Mach 1.94) crossflows were explored using traditional shadowgraphy and laser sheet illumination techniques, as well as a phase Doppler particle analyzer (PDPA). A compilation was made of recent attempts to correlate penetration height of a spray to various injection parameters. The compiled correlations for pure-liquid jets in subsonic crossflows are listed below, along with the new PDPA-derived correlations:

Table 1: Historical correlations for pure-liquid jets in subsonic crossflows

Year	Author(s)	Correlation	Method	
1969	Geery and Margetts	$\frac{h_0}{d_0} = 2.0 * q_0^{0.53} * \left(\frac{x}{d_0}\right)^{0.27}$	Motion frozen photography	**Eq. 5**
1993	Chen et al.	$\frac{h_0}{d_0} = 9.91 * q_0^{0.44} * \left(1 - e^{-(x/d)/13.1}\right) * \left(1 + 1.67 * e^{-(x/d)/4.77}\right)\left(1 + 1.06 * e^{-(x/d)/0.86}\right)$	Laser sheet illumination	**Eq. 6**
1997	Wu et al.	$\frac{h_0}{d_0} = 4.3 * q_0^{0.33} * \left(\frac{x}{d_0}\right)^{0.33}$	PDPA	**Eq. 7**
2002	Lin et al.	$\frac{h_0}{d_0} = 2.42 * q_0^{0.48} * \left(\frac{x}{d_0}\right)^{0.24}$	Shadowgraphy	**Eq. 8**
2002	Lin et al.	$\frac{h_0}{d_0} = 3.17 * q_0^{0.33} * \left(\frac{x}{d_0}\right)^{0.40}$	PDPA	**Eq. 9**

The correlations for pure-liquid jets in supersonic crossflows are as follows:

Table 2: Historical correlations for pure-liquid jets in supersonic crossflows

Year	Author(s)	Correlation	Method	
1972	Yates	$\frac{h_0}{d_0} = 1.15 * q_0^{0.5} * \ln\left(1 + 6 * \left(\frac{x}{d_0}\right)\right)$	Direct-lighting photography	**Eq. 10**
1978	Baranovsky and Schetz	$\frac{h_0}{d_0} = 1.32 * q_0^{0.5} * \ln\left(1 + 6 * \left(\frac{x}{d_0}\right)\right) * \sin\left(\frac{2}{3}\theta\right)$	Long-exposure photography, short-duration Schlieren	**Eq. 11**
2002	Lin et al.	$\frac{h_0}{d_0} = 3.94 * q_0^{0.47} * \left(\frac{x}{d_0}\right)^{0.21}$	Shadowgraphy	**Eq. 12**

The correlations for aerated-liquid jets in subsonic crossflows are as follows:

Table 3: Historical correlations for aerated-liquid jets in subsonic crossflows

Year	Author(s)	Correlation	Method	
2002	Lin et al.	$\frac{h-h_0}{d_0} = 0.59 * q_0^{0.33} * \left(\frac{x}{d_0}\right)^{0.45} * GLR^{0.49} * M^{-0.56}$	Shadowgraphy	**Eq. 13**
2002	Lin et al.	$\frac{h-h_0}{d_0} = 0.9 * q_0^{0.34} * \left(\frac{x}{d_0}\right)^{0.39} * GLR^{0.46} * M^{-0.64}$	PDPA	**Eq. 14**

Because of limitations with the PDPA equipment used in the studies of Lin et al.[10], accurate and reliable data could not be obtained in the supersonic environments, due to the inability of the PDPA equipment to measure the high-velocity particles.

Lin et al.[10] discovered that traditional imaging techniques, such as shadowgraphy and laser sheet illumination under-predicted the penetration height of the spray plume by up to 43% for pure-liquid jets in subsonic flows, and up to 35% in supersonic flows. The PDPA system was again used to investigate the spray plumes by Lin et al.[11], and it was discovered that the structure of the spray plume transitioned from concentric to horseshoe-shaped once aeration was added. It was hypothesized that the horseshoe-shaped liquid distribution was a result of the freestream vortical motion, which is induced by the increased blockage of the plume. Lin et al.[11] also observed that the droplet size decreased as GLR and freestream Mach number increased. It is hypothesized that the increased aeration enhances atomization and that the increased freestream Mach number imparts greater momentum to the liquid column ligaments exiting the injector, thus enhancing liquid column breakup. According to their data, there appears to be no significant effect of the jet-to-air momentum flux ratio to droplet size. It was found that SMD is fairly constant beyond $x/d_0=50$, suggesting that the atomization process was complete upstream of this axial location. Thus, aeration can fully atomize the liquid spray in a

relatively short axial distance. Finally, it was observed that the cross-sectional area of the plume increased with GLR, q_0, and x/d_0 and decreased as freestream Mach number increased.

In a first of its kind use of a two component phase Doppler particle analyzer, Lin et al.[12] probed an aerated-liquid spray in a Mach 1.94 supersonic crossflow, with water as the test injectant. In this study, it appeared that atomization processes were completed at $x/d_0<100$ and that SMD was fairly constant beyond $x/d_0=100$ on the order of 10 μm. Concurrently, Sallam et al.[14] reexamined the primary breakup of aerated-liquid jets in a supersonic crossflow using single- and double-pulsed shadowgraphy and holography. It was found that for finite aeration levels, the cone angles and surface breakup properties were similar on the upstream and downstream sides of the jet, suggesting a weak aerodynamic effect from the crossflow. Ligament and droplet sizes after primary breakup are relatively constant and independent of injector orifice size, GLR, q_0, or liquid properties for finite aeration levels. The average droplet diameter as measured in these studies was on the order of 40 μm.

To further the knowledge of aerated-liquid injection and enable better design data for future work, the current study investigates the spray plumes of aerated-liquid injectors and derives correlations for penetration height based on a number of design and injection parameters. Penetration height of the spray plume is vital, due to the large amount of momentum that can be dissipated by the boundary layer. The study uses shadowgraphy and laser sheet illumination techniques to establish a baseline similarity between the current study and past work, then employs the use of modern PDPA equipment to better characterize the spray plume. The derived correlations will allow more detailed designs of aerated-liquid injectors with more predictable spray characteristics.

EXPERIMENTAL SETUP

Experiments were carried out inside Test Cell 19 of the Air Force Research Laboratory, Wright-Patterson Air Force Base. Liquid injectors were flush mounted on the bottom plates of the high-speed wind tunnel. A complete description of the supersonic wind tunnel in Test Cell 19 was presented by Gruber et al.[15] This facility is a continuous-run, open-loop, rectangular supersonic wind tunnel with a height of 127 mm, width of 152 mm, and length of 762 mm. There are three quartz windows installed on the top and both sides of the test section to provide optical access. A series of compressors capable of providing up to 15 kg/s of air, with total pressures and temperatures up to 4.9 MPa and 920 K, respectively, supply air to the facility. For this series of experiments, total temperature was kept at 500 °F (533 K). An exhaust system lowers and maintains the backpressure for smooth starting and safe operation. A supersonic nozzle with performance Mach number of 1.94 is installed to provide a supersonic air stream. Air pressures and temperatures are measured using strain gauges and k-type thermocouples. Figure 2 shows a schematic of the wind tunnel.

A plain-orifice aerated-liquid injector, consisting of an internal tube for liquid flow and an external tube for aerating gas flow was flush mounted on the bottom plate of a supersonic wind tunnel to provide normal and angled injection. Figure 3 shows a schematic of the assembled injector. Injection angles of 45°, 60°, 75° and 90° (normal) were tested. The aerating gas flowed through the annular region between inner and external tubes and then passed through several small orifices (250 μm diameter) to mix with the liquid. Three interchangeable nozzles with orifice diameters of 0.5mm (0.020”), 1.0mm (0.040”), and 1.5mm (0.060”) were tested for each injection angle to investigate the effects of nozzle diameter on the structure of aerated-liquid jets. The nozzle passage length to the injector diameter ratio (L/d_0) was kept constant at

L/d_0=8 for each adapter. Nitrogen was used as the aerating gas throughout the test program. Even though flammable gases, such as hydrogen and ethylene, can be good candidates for aerating gas and have the capability for combustion enhancement, they were not used in the test series, due to safety requirements.

The liquid and aerating gas injection system consisted of a large liquid tank, two flow meters, and a nozzle unit. A schematic of the liquid supply system is included (see Figure 4). The injection tank had an internal volume of 0.144 m^3 and is rated for 3 MPa. The relatively large volume of the injection tank ensured a constant liquid supply pressure. Test liquids were filled into the liquid tank and pressurized with high-pressure nitrogen before each experiment. Liquid and aerating gas volumetric flow rates were controlled by pressure regulators and measured by flow meters. The flow meters were calibrated to an uncertainty of less than 2%. Measured liquid volumetric flow rates were used to derive liquid injection velocities based on the nozzle exit diameter.

Spray penetration height measurement and spray visualization were performed using shadowgraphs. A CCD camera (Redlake ES4.0); Epix, Inc., PC interface card and software (Xcap) was used to record images. Laser sheet illumination was utilized to visualize the spray cross-sectional structure. A laser sheet with a height of 50 mm and a thickness of about 200 μm intersected the spray at a 90-degree angle from the side. The light scattered from droplets within the spray plume was captured by the Redlake ES4.0 CCD camera, which was positioned at an angle from the freestream air and was facing upstream; images were then corrected for perspective distortion using a reference image (a dotcard with 0.25” dot spacing). Location of the laser sheet relative to the injector exit was varied between 5 to 200 diameters downstream the injector and 50 images of the light scattered by the droplets were captured at each location. A

frequency-doubled Nd:YAG laser with a wavelength of 532 nm and a pulse duration of 10 ns was used as the light source for these measurements. The short laser pulse duration was sufficient to freeze the motion of the liquid column and the droplets. The entire optical setup was mounted on an optical table capable of traversing in all three dimensions in order to accommodate the rigidly mounted wind tunnel. The traversing system has a positioning accuracy of 0.1 mm.

A two-component phase Doppler particle analyzer (PDPA), along with a 5-W argon iron laser and a TSI FSA4000 burst correlator, was also used to determine properties of droplets and spray plumes. The clear aperture and focal length of the transmitter were 50 and 500 mm, respectively. The initial beam diameter was 1.77 mm. Beam separation was 20 mm. A beam expander with an expansion ratio of 2 was used to reduce the size of the probe volume. The waist diameters of the probe volume for 488- and 514.5-nm wavelengths were 91.4 and 92.5 μm, respectively. The receiver has a clear aperture of 106 mm in diameter and a collecting lens with a focal length of 370 mm. The collected light was passed through a 25-μm slit to further reduce the probe volume. Light was collected at 30° from the transmitter (refractive scattering). Droplet size, axial velocity, and volume flux were measured in the transverse and spanwise directions across the spray plume. Measurements were performed at several downstream locations, i.e., x/d_0=10 to 200. A spatial increment of 1.27 mm was used for measurement in the cross stream (z) direction and an increment of 1.27 or 2.54 mm was employed for measurement in the jet injection (y) direction, depending on the spray structure. Regions with unbroken liquid core, irregular ligaments, and non-spherical drops, where PDPA measurements can not be carried out reliably, were avoided for the determination of detailed structures of the entire cross-sectional area. For penetration height measurement, the edge of the spray plume was probed,

even though the entire spray structure is not suitable for detailed PDPA measurement. For spray plume areas with high number density, droplet properties were averaged over more than 30,000 droplets at each location to reduce the experimental uncertainties. Otherwise, a constant duration of 10 seconds was used for data acquisition. Measurements were stopped when the measured liquid volume flux was below 0.01 cc/s/cm^2. Matrices detailing the test conditions explored are below:

Table 4: Test conditions for shadowgraphy. Jet-to-air momentum flux ratio (q_0) is given as a ratio and gas-to-liquid mass ratio (GLR) is given in percentage.

		d_0=0.02”								d_0=0.04”								d_0=0.06”							
θ=45°	q_0=	3	7	10	14	3	3	3	3	5	3	6	10	15	6	3	3	4	3	6	1	1	3	3	3
	GLR=	0	0	0	0	3	5	7	10	3	0	0	0	0	1	3	5	4	0	0	0	4	1	2	3
θ=60°	q_0=	3	7	10	14	3	3	5	7		3	6	10	15	3	3	4		3	6	1	1	3	3	3
	GLR=	0	0	0	0	3	5	5	2		0	0	0	0	3	5	3		0	0	0	4	1	2	3
θ=75°	q_0=	3	7	10	14	3	3	3	3	5	3	6	10	15	3	3			3	6	1	1	3	3	3
	GLR=	0	0	0	0	3	5	7	10	3	0	0	0	0	3	5			0	0	0	4	1	2	3
θ=90°	q_0=	3	7	10	14	7	3				3	6	10	15	3	3	4		3	6	1	3	3	3	1
	GLR=	0	0	0	0	2	5				0	0	0	0	3	5	4		0	0	0	1	2	3	4

Table 5: Test conditions for laser sheet illumination. Jet-to-air momentum flux ratio (q_0) is given as a ratio and gas-to-liquid mass ratio (GLR) is given in percentage.

		d_0=0.02”							d_0=0.04”					d_0=0.06”				
θ=45°	q_0=	3	7	14	3	3	3	7										
	GLR=	0	0	0	3	5	7	5										
θ=60°	q_0=	3	7	14	3													
	GLR=	0	0	0	7													
θ=75°	q_0=	3	3	3														
	GLR=	0	5	7														
θ=90°	q_0=	3	7	14	3	3	3	3	3	7	3	7	10	3	3	1	3	7	3	3
	GLR=	0	0	0	3	5	7	4	8	2	0	0	0	3	5	0	0	0	3	1

Table 6: Test conditions for phase Doppler particle analyzer (PDPA). Jet-to-air momentum flux ratio (q_0) is given as a ratio and gas-to-liquid mass ratio (GLR) is given in percentage. Test conditions listed in red were used for plume cross-section measurements while test conditions listed in black were used for penetration height measurements.

		d_0=0.02”	d_0=0.04”	d_0=0.06”
θ=45°	q_0=	7 | 7 | 3	3 | 2	
	GLR=	0 | 5 | 7	0 | 7	
θ=60°	q_0=	14 | 3 | 5 | 6	5 | 4	
	GLR=	0 | 5 | 5 | 2	0 | 3	
θ=75°	q_0=	3 | 10 | 3 | 5	4 | 7	
	GLR=	0 | 0 | 7 | 3	0 | 1	
θ=90°	q_0=		7	
	GLR=		0	

RESULTS AND DISCUSSION

Shadowgraphy Results

To obtain a penetration height measurement from the shadowgraph imagery, an intensity profile was taken at locations of x=2.54 mm (0.1”), 5.08 mm (0.2”), 12.7 mm (0.5”), 25.4 mm (1.0”), and 50.8 mm (2.0”) using a Matlab script (see Appendix A). These axial locations corresponded to those at which laser sheet illumination images were recorded, allowing for direct comparisons at each axial station between the two penetration height predictions. To measure the spray penetration height from the shadowgraph images, the average background intensity value (I_0) was calculated from a rectangular region above the spray plume and behind the dark region in the left-hand side of every image, in order to calculate the most representative background intensity without the interference of undesired noise, such as shock patterns, dirt, scratches, and condensation. An example shadowgraph image showing this rectangular region is shown in Figure 5. The intensity profile at each x location was then normalized by the average background intensity. However, certain background artifacts still remained and had the effect of offsetting the background value for I/I_0 from unity. To compensate, I/I_0 was further normalized by the average value of I/I_0 where the curve asymptotically approached a constant linear value. This asymptotic value was found by visual inspection of the intensity profile. The boundary of the spray plume was assumed to be where the intensity value was 90% of the background intensity, or when $I/I_0=0.9$. An interesting result of using the average value of I/I_0 is that the actual mean value of the background intensity no longer matters for penetration height measurements. Because the intensity is then normalized by the average value of the asymptotic region, the same penetration height is obtained regardless of whether the mean intensity value is changed. The penetration height correlations were found by finding a linear fit of the powers on

each term. The base 10 logarithm of each term was found and, using a linear fit algorithm in Microsoft Excel®, the power for each term was calculated.

Figure 6 is an example of shadowgraph imagery obtained in this study. The progression of images compares the effects of injection angle, θ, as well as overlaying the penetration height predicted by the various correlations derived in this study. These figures indicate that increasing the injection angle towards normal injection enhances spray penetration, which agrees well with past observations. Data gleaned from the shadowgraph imagery resulted in the following correlation for pure liquid jets:

$$\frac{h}{d_0} = 0.018 * (1 + \sin(\theta))^{6.0} * \left(\frac{x}{d_0}\right)^{0.40} * q^{0.63} \qquad \textbf{Eq. 15}$$

Figure 7 shows the effect of increasing d_0 on spray penetration height for jets with θ=90°, q_0=3, and GLR=0. As d_0 increases, the spray plume penetrates further into the core flow. The increase in cross-sectional area of the orifice allows more mass to flow though and thereby increases the overall effective momentum of the jet. Finally, the effect of increasing the momentum flux ratio of the water spray can be seen in Figure 8. As q_0 increases, h/d_0 also increases slightly. However, as can be seen from the figure, the correlation over-predicts the influence of the liquid jet momentum flux on penetration height beyond $x/d_0 \approx 25$.

The correlation for aerated-liquid jets as derived from the shadowgraph images was found to be:

$$\frac{h}{d_0} = 0.51 * (1 + \sin(\theta))^{2.6} * \left(\frac{x}{d_0}\right)^{0.33} * q_0^{0.23} * GLR^{0.099} \qquad \textbf{Eq. 16}$$

In previous work, correlations accounted for spray angle by the inclusion of a sin(θ) term. It was found in this study that a better correlation could be arrived at by introducing the

spray angle term as (1+sin(θ)). This allows the angle term in the correlation to always be non-zero, which allows this correlation to be used for injection angles close to and at parallel to the freestream. However, it is assumed that injection angles close to parallel to the freestream will result in different spray characteristics, since there would be a considerable amount of freestream momentum acting in the same direction as the spray momentum.

In an effort to characterize the spray plume penetration height in one correlation, incorporating both pure- and aerated-liquid jets, a new correlation was found in which the GLR term was replaced with (100+GLR), which allows the correlation to be used with pure-liquid jets because the term is always non-zero. The choice of the constant added to the GLR term is consistent with the use of GLR in percentage. Therefore, a gas-to-liquid mass ratio of 3% would translate to (100+3) in the GLR term of the correlation. The unified shadowgraph-derived correlation is found below:

$$\frac{h}{d_0} = 0.071*(1+\sin(\theta))^{4.6}*\left(\frac{x}{d_0}\right)^{0.35}*q_0^{0.42}*(1+GLR)^{0.40} \qquad \textbf{Eq. 17}$$

In Eq. 16 and Eq. 17 GLR is in percentage. Figure 9 shows the effect of increasing GLR in the spray penetration height. While increasing GLR seemingly has little effect on the penetration height of the spray in these shadowgraph images, PDPA measurements suggest that penetration height is greatly affected by the amount of aeration, as will be discussed later. The unified shadowgraph correlation seems to be a poor match at low injection angles and high values of GLR. However, the unified correlation seems to better match the asymptotic behavior of the spray plume as it moves further downstream. Physically, it is intuitive that the spray plume will cease to grow in height at some finite point downstream where aerodynamic drag forces and gravity have dissipated the vertical spray momentum imparted at the injection site.

The combined data used to formulate the correlations for pure liquid jets and aerated-liquid jets in a supersonic crossflow are plotted in Figure 10 through Figure 13. As can be seen from the graphs, the penetration height correlation is much closer to experimental results for the aerated-liquid jets than for the pure-liquid jets in all cases. As can be seen from these figures, there is an extreme outlying data point corresponding to the 45° angled pure-liquid (GLR=0%) injection with a 0.5 mm orifice diameter, and jet-to-air momentum ratio (q_0) of 3. Because of the low angle of injection and jet momentum in this particular case, it can be reasonably assumed that the boundary layer along the test section floor dissipated much of the jet momentum, resulting in a lower measured penetration height than the correlation predicted. Future work should either investigate the effects on the spray plume if the boundary layer influence is removed, possibly accomplished by boundary layer bleed through a porous floor, or investigate the use of a boundary layer correction factor.

Laser Sheet Illumination Results

Due to the unsteady nature of the spray plume in the transverse direction, the 50 laser sheet illumination images from each x location were averaged together. An example of this unsteady phenomenon can be seen in the progression of images in Figure 14. Note that a reflection of the spray plume can be seen in the lower center portion of each image and should not be considered any portion of the spray itself. Appendix A contains the Matlab code used to perform this and other transformations on the laser sheet imagery. For the measurements of spray penetration height and plume width, a linear transformation was applied to the averaged images, in which a dotcard pattern of known dimensions was used as a reference to correct for the skewness of the images due to the offset angle of the camera. Figure 15 shows an example of the original dotcard image, the unskewed dotcard image, and a sample of a skewed and

unskewed spray plume image. Note that there is negligible change in the overall size and shape of the spray plume. The measured change in height and width of the spray plume due to the unskewing of the image was less than 1% in either direction. Also note that the bottom of the image is transported to the top in the unskewed images. This is due to the unskewing algorithm relocating the pixels so that no image information is lost in the transformation. These pixels were measured to be below the injection orifice, and therefore could be ignored. These images were then converted to black and white images using a consistent gray-level threshold value of 2.5% of the total gray-level range (65,536 in the case of 16-bit images, 256 in the case of 8-bit images). This level was found through inspection to eliminate background noise while enhancing the contrast of the spray plume and revealing low-intensity level droplets on the fringes.

Figure 16 shows an image converted from intensity (grayscale) to black and white. The figure shows that much of the spray plume was invisible to the naked eye due to the small, low-intensity droplets at the fringes of the plume. A sensitivity analysis was performed on the choice of intensity level to determine the effect of changing this value on penetration height and spray plume width measurements. The intensity value was reduced by half (to 1.25%) and doubled (to 5%) and new measurements for height and width were taken for a representative sample of images. Figure 17 shows the results of the sensitivity analysis graphed against x-location. It was found that halving the intensity value in the conversion to black and white imagery produced an average 18% increase in penetration height and 45% increase in spray plume width. However, the background horizontal scan lines from the camera's photoreceptors became visible at the edges of the spray plume at this decreased intensity threshold and therefore skewed the width results considerably. It was also found that doubling the intensity value produced an average

15% decrease in penetration height and 32% decrease in spray plume width. At this high intensity threshold, some of the image data was lost completely at the furthest downstream x locations, particularly for the aerated-liquid jets. The low intensity level light reflected from these small droplets is below the intensity threshold at 5% intensity. From the black and white imagery, the boundary of the spray plume was found and the penetration height was measured directly through visual inspection. Again, as with the shadowgraph images, correlations were computed using a linear fit of the power of each term.

Similar to observations made in the shadowgraph imagery, increasing the injection angle toward normal injection increases the penetration height of the spray plume (see Figure 18). It can also be seen from these images that there is a large concentration of liquid spray in the center of the plume, which penetrates farther from the wind tunnel floor as angle increases (note high intensity region at the top of each spray plume). Figure 19 shows the effect of increasing the liquid spray momentum flux on the penetration height and width. These images show much the same trend as the shadowgraph imagery (see Figure 8). However, of note in the laser sheet illumination imagery is that momentum flux seems to have little effect on the spray plume width. This is to be expected because the momentum is almost exclusively in the z-direction when injected.

In Figure 20, the effect of increasing the liquid aeration is seen. Unlike the shadowgraph imagery, theses images do show an increase in penetration height as GLR is increased, as well as an increase in spray plume width. It is worthwhile to note that the horseshoe shape present in previous studies by Lin et al.[12] is also observed here. However, when investigating imagery from test conditions using the 1.5 mm diameter injector orifice, the horseshoe structure of the

spray plume could not be seen, since these sprays are too dense for laser light to pass through to expose the cross-sectional structures.

The following correlations were found for h/d_0 and w_s/d_0 for pure liquid jets:

$$\frac{h}{d_0} = 0.068*(1+\sin(\theta))^{5.4}*\left(\frac{x}{d_0}\right)^{0.38}*q_0^{0.38} \quad \textbf{Eq. 18}$$

$$\frac{w_s}{d_0} = 2.3*(1+\sin(\theta))^{0.011}*\left(\frac{x}{d_0}\right)^{0.44}*q_0^{0.016} \quad \textbf{Eq. 19}$$

The following correlations were found for h/d_0 and w_s/d_0 for aerated-liquid jets:

$$\frac{h}{d_0} = 1.5*(1+\sin(\theta))^{1.8}*\left(\frac{x}{d_0}\right)^{0.29}*q^{0.23}*GLR^{0.032} \quad \textbf{Eq. 20}$$

$$\frac{w_s}{d_0} = 2.9*(1+\sin(\theta))^{0.27}*\left(\frac{x}{d_0}\right)^{0.24}*q^{0.17}*GLR^{0.17} \quad \textbf{Eq. 21}$$

In Eq. 20 through Eq. 23 GLR is in percentage. As with the shadowgraph-derived correlations, the data from the laser sheet illumination imagery for pure- and aerated-liquid jets was also combined to formulate a unified correlation for penetration height and spray plume width, given below:

$$\frac{h}{d_0} = 0.51*(1+\sin(\theta))^{2.9}*\left(\frac{x}{d_0}\right)^{0.23}*q_0^{0.37}*(1+GLR)^{0.24} \quad \textbf{Eq. 22}$$

$$\frac{w_s}{d_0} = 8.0*(1+\sin(\theta))^{-0.31}*\left(\frac{x}{d_0}\right)^{0.093}*q_0^{0.16}*(1+GLR)^{0.15} \quad \textbf{Eq. 23}$$

These correlations are plotted versus the various test parameters in Figure 21 through Figure 28. Although it seems that the correlations have a wide margin of error, it can be seen from Figure 24 and Figure 28 that it is the pure-liquid injection cases where the correlations are most unreliable. All of these graphs show that the aerated-liquid correlations derived from the

laser sheet illumination imagery are the most accurate at predicting penetration height and spray plume width.

Phase Doppler Particle Analyzer Results

The method described in the experimental setup was used to obtain measurements for penetration height using the phase Doppler particle analyzer (PDPA). Two correlations for the penetration heights of pure- and aerated-liquid jets are derived from the combined PDPA measurements in the present study and in the study by Lin et al.[12] for normal injection. To validate the current test setup against previous measurements taken with PDPA equipment, several test conditions investigated by Lin et al.[12] in 2002 were repeated and found to match almost precisely. The obtained correlations are as follows:

For the pure-liquid jets:

$$\frac{h_0}{d_0} = 0.98 * (1+\sin(\theta))^{2.1} * \left(\frac{x}{d_0}\right)^{0.33} * q_0^{0.31} \qquad \textbf{Eq. 24}$$

For the aerated-liquid jets:

$$\frac{h_0}{d_0} = 0.98 * (1+\sin(\theta))^{1.65} * \left(\frac{x}{d_0}\right)^{0.40} * q_0^{0.38} * GLR^{0.27} \qquad \textbf{Eq. 25}$$

As with the previous two techniques, a third correlation for the penetration height was derived, replacing the GLR term with (1+GLR) in order to combine the pure- and aerated-liquid jets into one correlation, which is below:

$$\frac{h}{d_0} = 0.99 * (1+\sin(\theta))^{1.8} * \left(\frac{x}{d_0}\right)^{0.37} * q_0^{0.33} * (1+GLR)^{0.28} \qquad \textbf{Eq. 26}$$

These correlations were computed using the same linear power fit as the correlations derived from shadowgraphy and laser sheet illumination imagery. These correlations are plotted

against the test parameters in Figure 31 through Figure 34. Figure 33 and Figure 34 especially show the accuracy of these three correlations. Most of the correlation predictions fit within 10% of the measured penetration heights, suggesting that the PDPA data and the PDPA derived correlations are more accurate for defining and predicting spray plume penetration height than the previous two techniques. Because the PDPA equipment is capable of detecting much smaller droplets in areas of low concentrations, it is expected that this would be the case. Figure 29 shows a comparison between the correlations for penetration height derived from this study and historical correlations for pure-liquid jets in supersonic crossflow. The correlations by Yates (1972) and Baranovsky and Schetz (1978) under-predict the penetration height by up to 83.3% and 83.7%, respectively and the correlation by Lin et al. (2002) under-predicts the penetration height by up to 55.5% in the region of $x/d_0 \leq 100$.

Figure 30 shows a comparison of sample laser sheet illumination imagery to PDPA measurements. Because the amount of laser light reflected by the plume is directly related to the droplet number density in the spray plume, the laser sheet illumination images are compared to plots of the droplet number density as measured by the PDPA system. While the laser sheet images appear to pick up most of the general features of the spray plume, they fall short of characterizing the fine details captured by the PDPA system. However, it should be noted that the PDPA system took measurements over a short interval at each y, z location while the laser sheet images were averaged from 50 consecutive shots. This discrepancy in the techniques used to generate imagery makes it difficult to perform a true comparison of the resulting data.

Applications for Scramjet Operation

The results of the work by Mathur et al.[6] show promise that JP-7 is a viable fuel for scramjet operations. Work done by Sallam et al.[14] suggests that, though the physical properties

of JP-7 and water are vastly disparate, the physical properties of the injectant liquid seemingly have little effect on the atomization processes inside an aerated-liquid injector, and therefore the results obtained from studies using water as the test injectant can be readily applied to JP-7. In an effort to characterize the actual performance of the aerated-liquid injector in a scramjet combustor, the PDPA measurements of volume flux in the spray plume cross-section were used to estimate a local equivalence ratio, based on the density of liquid JP-7 at 298K. A global equivalence ratio was calculated using the volumetric flow rate of the liquid as measured from the liquid flow meters, multiplied by the density of liquid JP-7, and the mass flow rate of air through the wind tunnel, as calculated from the known total temperature and pressure. To determine the mass flow rate of air at the spray plume site in the tunnel, isentropic relations were used to calculate flow properties downstream of the facility nozzle and oblique shock relations were used to calculate the flow properties behind the bow shock upstream of the injector orifice. Several assumptions were made which make these local equivalence ratios only accurate to a rough order of magnitude. Among these assumptions is a neglect of the blockage of the freestream flow created by the spray plume itself, and an assumption that the oblique bow shock coming from the spray plume is two dimensional. There is also no accounting for boundary layer effects or skin friction slowing of the freestream flow. Finally, due to the relatively small amount of time a droplet travels from injector orifice to the downstream measurement site compared to the evaporation time, droplet evaporation is neglected. Sample calculations of 30-40 μm diameter droplet evaporation times put these times at more than 20 times the time of flight of a droplet.

Figure 35 shows the plots of local equivalence ratios for six test conditions where PDPA measurements were taken across the cross-section of the spray plume. Because the local

equivalence ratio at each point in the plume was normalized by the global equivalence ratio, the scale to the side of each image represents a multiple of the global equivalence ratio. Therefore, as can be seen in the images, local equivalence ratios inside the dense sections of the spray plume may reach over 100 times the global equivalence ratio. However, it is useful to note the average Sauter Mean Diameter (SMD) of the droplets in these regions is typically on the order of 10-20 μm. From Eq. 1, droplet burning time for droplets with this diameter is calculated to be on the order of 0.1 to 0.5 thousandths of a second, giving ample time for complete combustion before exiting the combustion section.

SOURCES OF ERROR

The shadowgraph imagery was plagued by background noise and dirt that affected the background intensity levels. While efforts were made to eliminate this background noise as much as possible, some artifacts still remained which may have slightly skewed penetration height measurements.

In recording data for the laser sheet illumination imagery, 30% of the test conditions were recorded at 8-bits per pixel, while the rest were recorded at 16-bits per pixel. The 8-bit images contained less intensity information, which may have resulted in the removal of smaller droplets at the fringes of the spray plume when they were converted to black and white. This loss of boundary data would result in a smaller measured plume height and width. Another source of error from the laser sheet illumination technique is that the intensity of the laser was not increased as a function of x distance from the injection site. Because droplets sizes decreased and droplet scatter increased with increasing x distance, less laser light was scattered by the droplets and therefore received by the camera. Plume size measured beyond the x=1.0 in position was artificially small due to the low level of laser intensity recorded by the camera.

In all test conditions there was an oblique shock present in the flow approximately 12.7 mm downstream of the injector orifice centerline. This oblique shock was created by a step in the wind tunnel floor, measuring approximately 0.13 mm in height. In some of the data it is clear that this oblique shock interfered with the spray plume, particularly when the injection angle was low (θ=45°) and when the momentum flux of the jet (both pure liquid and aerated-liquid) was also low (q_0=3).

CONCLUSIONS

Comparisons were made of various techniques for visualizing the structures of pure- and aerated-liquid jets injected into a supersonic crossflow. Correlations were derived from the data for penetration height and spray plume width. These correlations can be used to more precisely design aerated-liquid injectors to create the desired spray plume characteristics. It was found that, because of its ability to detect smaller, less densely concentrated particles, the phase Doppler particle analyzer (PDPA) system better characterizes the spray plume in the area far downstream of the injector. However, because the spray plume is too dense to get accurate readings from the PDPA system in the areas close to the injection site (within ~100 x/d_0), the laser sheet illumination and shadowgraph data are better suited for characterizing the spray.

Because droplet evaporation time is on an order with the residence time in the combustor, it is vital to efficient combustion to atomize the fuel spray as quickly as possible. As can be seen from the data presented in this study, aeration of the spray provides adequate atomization to ensure that droplets are fully evaporated and burned before exiting the combustor.

Penetration height is one key design parameter of aerated-liquid injectors. It is necessary to ensure the liquid fuel spray is able to escape the boundary layer of the combustor wall and deliver sufficient amounts of fuel to the entire combustor cross-section. Gruber et al.[16] measured the boundary layer thickness at the injection site (approximately 5.875” downstream of the facility nozzle exit plane) to be approximately 0.2”. It can be seen from the imagery that this boundary layer thickness is a significant fraction of the penetration height of most of the sprays, particularly the pure-liquid jets. Furthermore, it can be seen from the PDPA imagery that if the spray does not have sufficient momentum to penetrate the boundary layer, much of the liquid is

trapped inside the boundary layer, where it is unable to mix properly with the freestream air for complete and efficient combustion.

From this study, it can be seen that spray penetration height can be enhanced by increasing any of the four parameters tested. Spray penetration height correlations derived from PDPA measurements offer the most accurate predictions of penetration height behavior, so it is suggested that these correlations be used in future designs. It is clear from the included figures of this study that more investigation needs to be performed into possible correction factors to account for boundary layer and bow shock interactions, particularly for the low injection angle and low momentum flux cases.

It was observed that normal injection produced the best penetration into the core flow of the wind tunnel. However, future work should investigate the potential of forward-angled injectors, i.e. $\theta>90°$ in this study's reference frame, to provide even greater penetration height at a smaller x/d_0. Because some of the aerated-liquid jet's momentum is acting counter to the freestream momentum and must therefore be overcome by the freestream before being blown downstream, the spray should achieve the same penetration height in less x distance.

Future work should also include a study to determine the amount of liquid entrained into a flameholding device typical of that implemented in current scramjet combustor designs, such as cavity-based flameholders. Such studies will examine the tradeoffs between spray penetration of the core flow and starving the flameholder of fuel. Either a balance between the two will need to be found or a hybrid fueling system requiring one set of injectors for core penetration and another for flameholder fueling will be needed. Furthermore, future studies should focus on using actual hydrocarbon fuels versus water, since liquid hydrocarbons vary physically from water in density, surface tension, viscosity, boiling point and other properties. While previous

studies have found that the physical properties of the liquid injectant seem to have little effect on the atomization process, any changes in density, which in turn affect mass, could potentially affect penetration height, since more momentum would be required to move a larger mass the same distance.

Sufficient studies have not yet been performed to determine whether more combustion efficiency is gained using a non-reacting aerating agent, a fueling aerating agent, or an oxidizing aerating agent. It is assumed that the use of a fuel or oxidizer will result in better efficiency over an inert gas; however, there is still debate over the benefits of using a fuel over an oxidizer to effervesce the liquid fuel. Using a fuel, such as gaseous hydrogen, may promote combustion because gaseous hydrogen is much easier and quicker to ignite than liquid hydrocarbons, therefore introducing the flame to the liquid spray faster. On the other hand, using an oxidizer, such as gaseous oxygen, creates a flammable mixture within the liquid spray plume itself, expediting combustion by reducing mixing times. A major disadvantage to using an oxidizer as an aerating agent is that, when combined with a hot liquid fuel, there is a large potential for coking.

Finally, more research should be conducted into the actual effects of these parameters presented here in this paper on combustion efficiency. In particular, few studies have been made on actual combustion processes in environments representative of those encountered in high supersonic to hypersonic flight. These studies may include more detailed investigations into the local equivalence ratios of the spray plume and a correlation of equivalence ratio to various injector design parameters. Until such studies are made, the effects of aerated-liquid injection are still only speculative.

It should be noted that the correlations derived in this study are somewhat deficient in that they do not account for different freestream Mach numbers or total temperatures. That is, these correlations have not been verified outside of the freestream conditions tested in this series of experiments. In addition to the previously mentioned future work suggestions, it is also recommended that future work determine the effect of varying freestream Mach number and total temperature, to include these parameters also in future correlations.

The results of this study provide useful data for detailed design of future pure- and aerated-liquid injectors for a variety of applications, particularly when injecting into a supersonic crossflow. Because of the wide variety of parameters investigated, injectors may now be designed to generate a specific spray plume size and shape, to a great degree of accuracy. In particular, this will allow future scramjet combustor designs to be fully optimized for combustion efficiency, paving the way for greater thrust-to-drag ratios and higher payload capacities.

Table 7: Useful properties of JP-7

Molecular Weight	0.1734 kg/mol
Density	0.792 Mg/m^3 at 298 K
Vapor Pressure	0.048 kPa at 298 K
Surface Tension	2.255 x 10^{-3} mN/m at 298 K
Kinematic Viscosity	1.775 mm^2/sec at 298 K
Autoignition Temperature	514 K at 1 atm
Flammability Concentration Limits (fuel vapors in air)	
(vol%)	0.6
Lower (lean) limit	4.6
Upper (rich) limit	
Stoichiometric Fuel/Air Ratio	0.06719
Heat Capacity (C_p)	2.025 kJ/(kg-K)

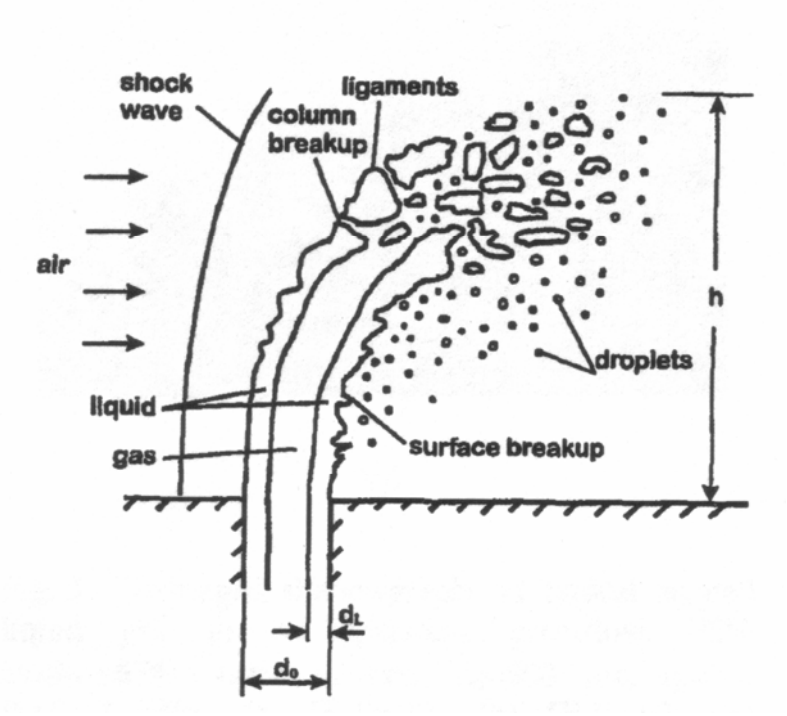

Figure 1: Typical aerated-liquid breakup process in a supersonic crossflow. (Reprinted here without permission.)

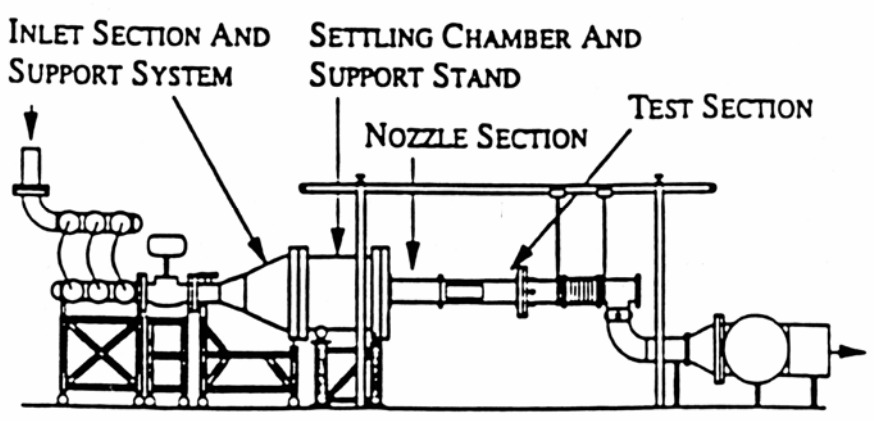

Figure 2: Schematic of AFRL/PRA Test Cell 19 supersonic wind tunnel facility

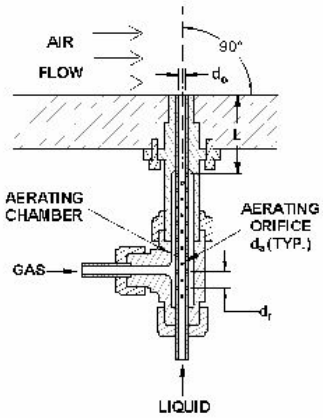

Figure 3: Aerated-liquid injector schematic (typical).

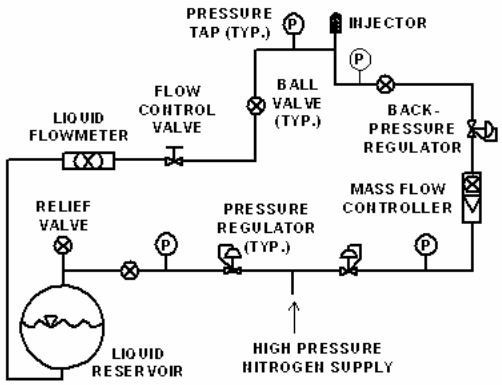

Figure 4: Schematic of liquid and aerating gas injection system

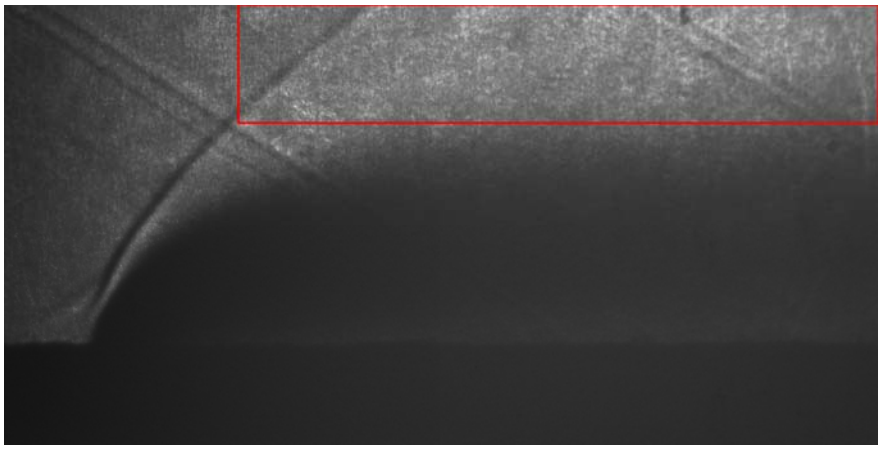

Figure 5: Typical shadowgraph image showing the rectangular region used to compute the average intensity value of the background.

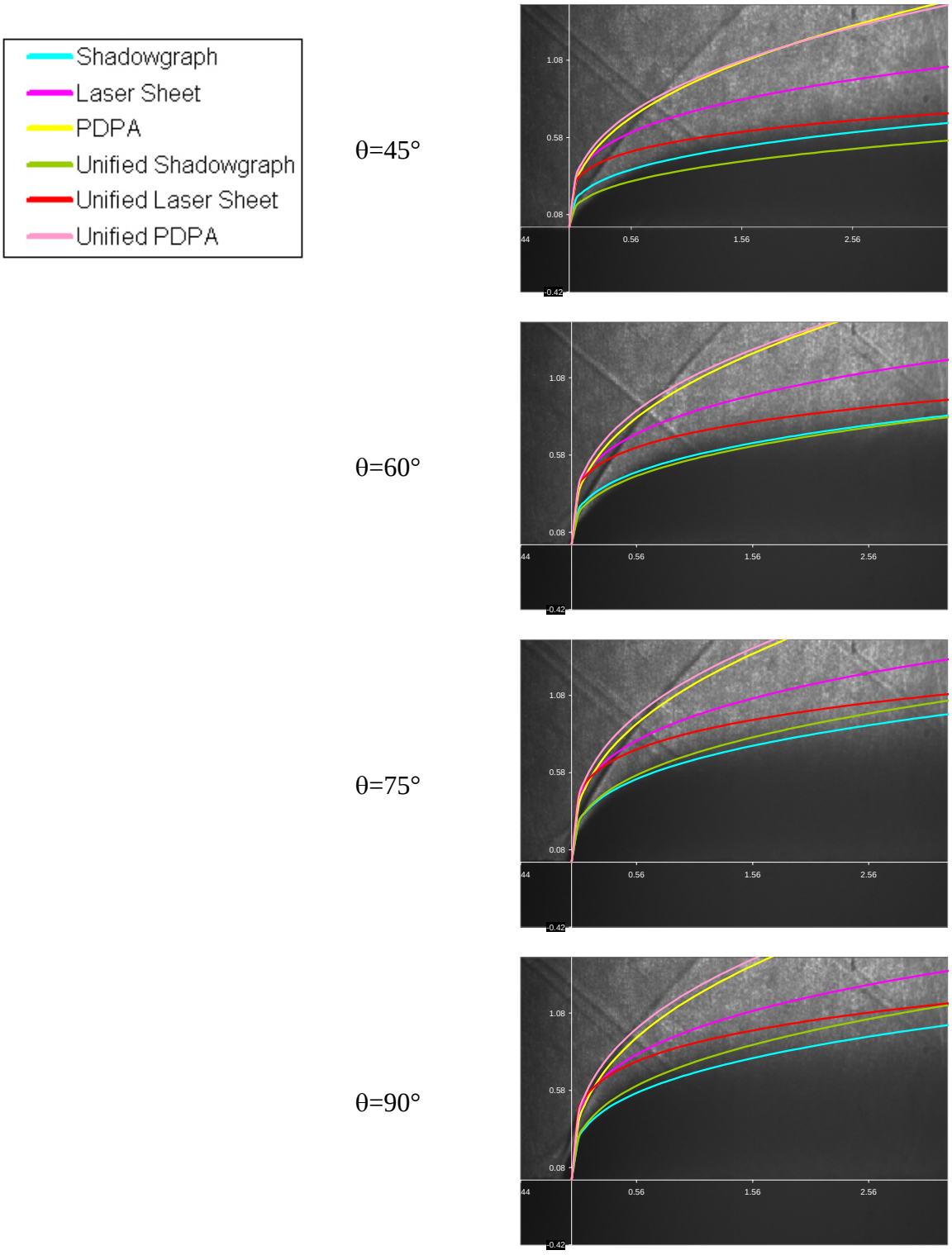

Figure 6: Shadowgraphy comparison of injection angles (θ). For these test conditions, d_0=0.060", q_0=3, and GLR=3%. Penetration height is measured on the y-axis and axial distance is measured on the x-axis, in inches.

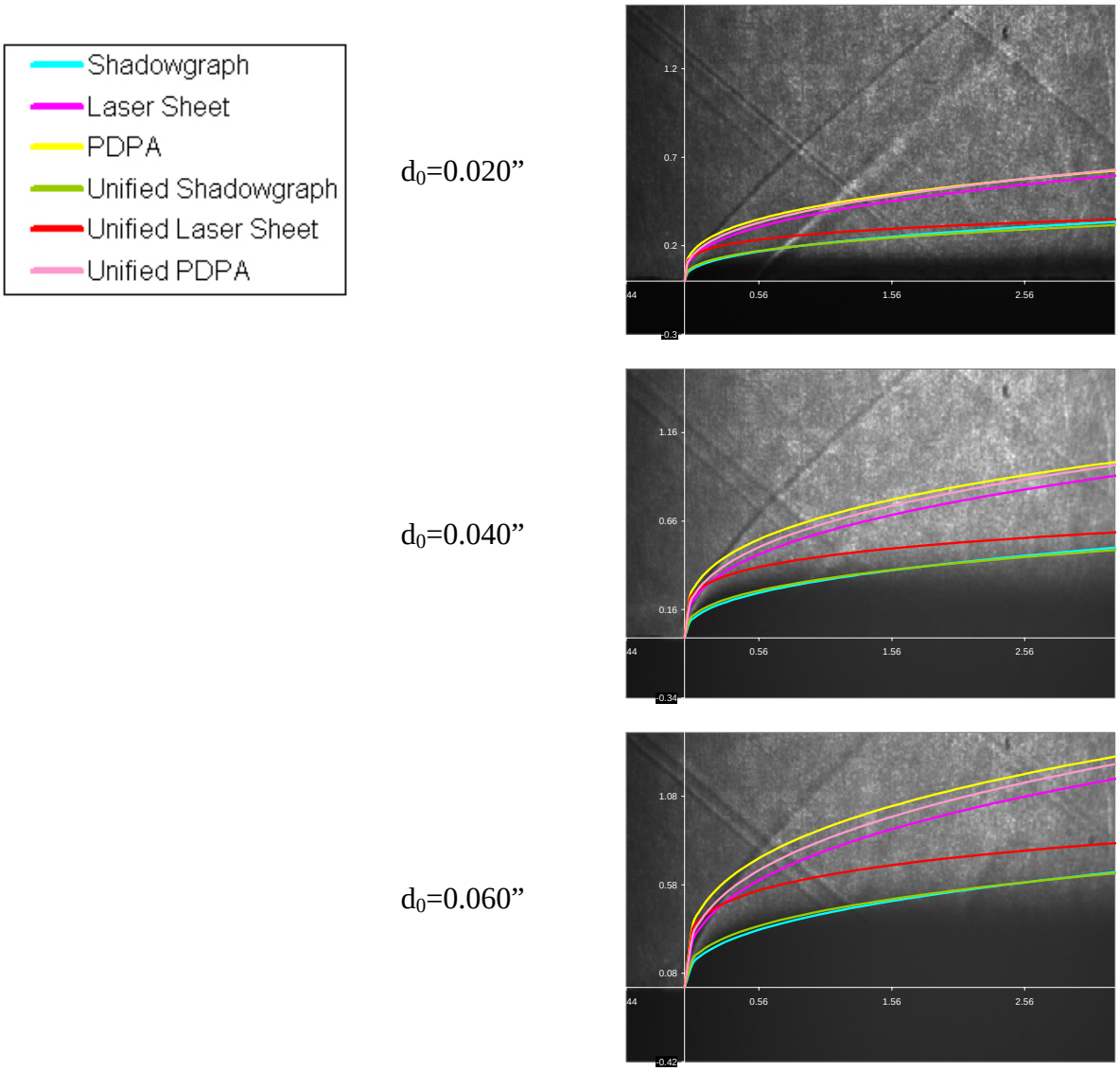

Figure 7: Shadowgraphy comparison of injection orifice diameters (d_0). For these test conditions, θ=90°, q_0=3, and GLR=0%. Penetration height is measured on the y-axis and axial distance is measured on the x-axis, in inches.

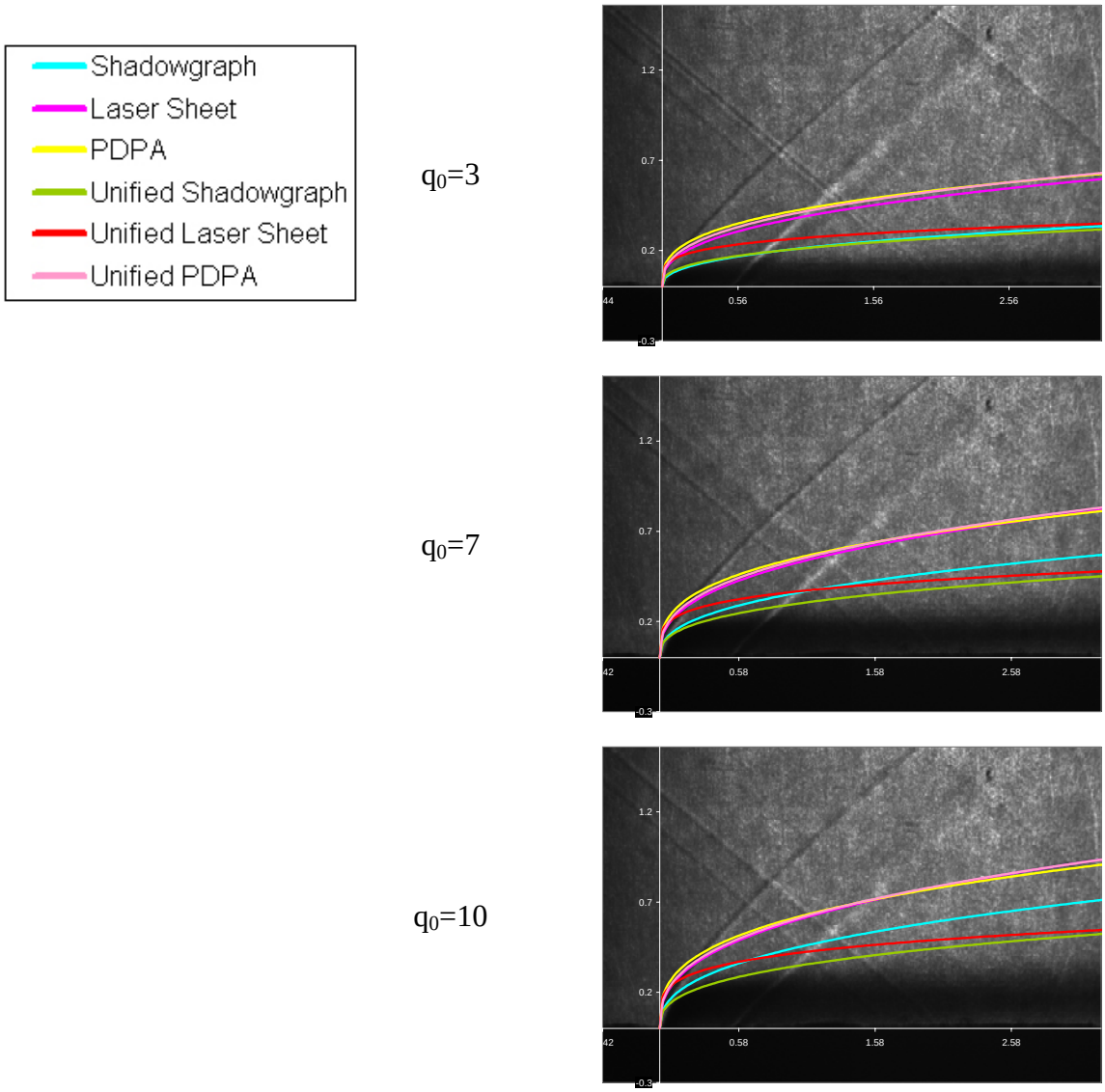

Figure 8: Shadowgraphy comparison of the effect of increasing jet-to-air momentum flux ratio (q_0). For these test conditions, θ=90°, d_0=0.020", and GLR=0%. Penetration height is measured on the y-axis and axial distance is measured on the x-axis in inches.

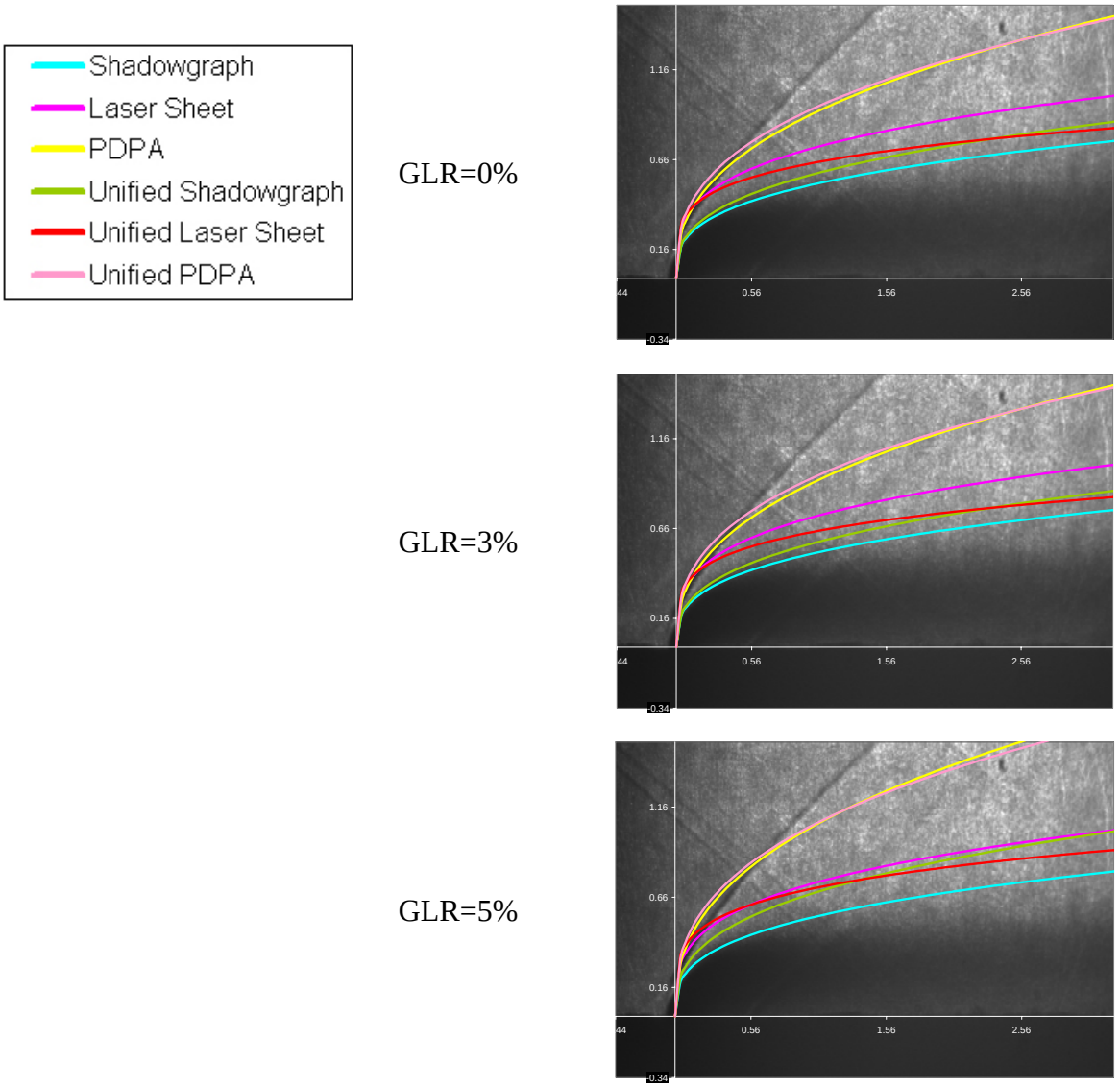

Figure 9: Shadowgraphy comparison of the effect of increasing gas-to-liquid ratio (GLR). For these test conditions, θ=90°, d_0=0.040", and q_0=3. Penetration height is measured on the y-axis and axial distance is measured on the x-axis, in inches.

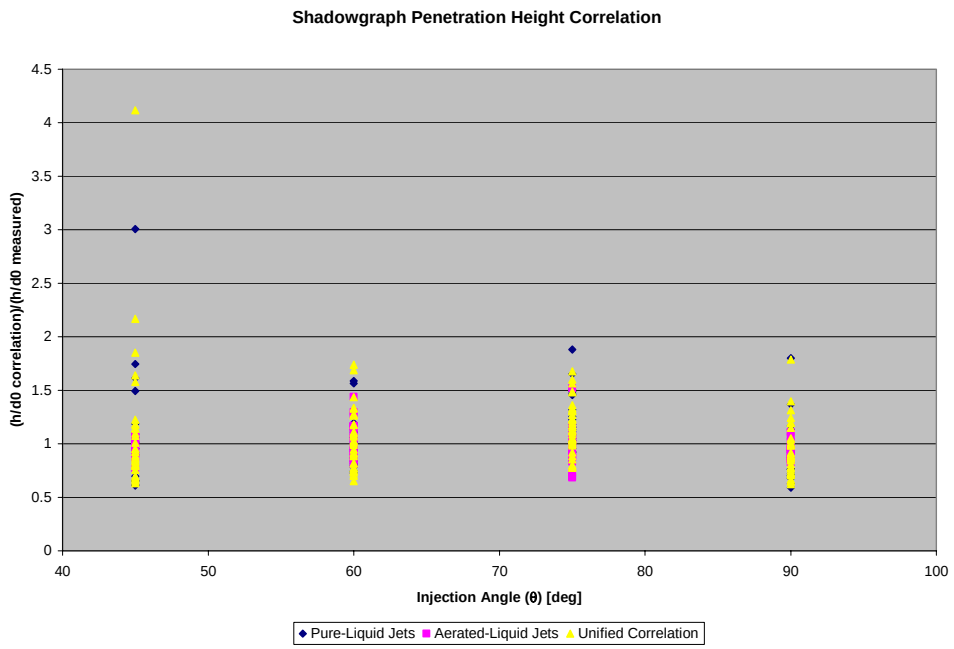

Figure 10: Spray penetration height correlation (h/d_0 correlation) derived from shadowgraphy, normalized by the measured penetration height (h/d_0 measured), graphed versus injection angle (θ).

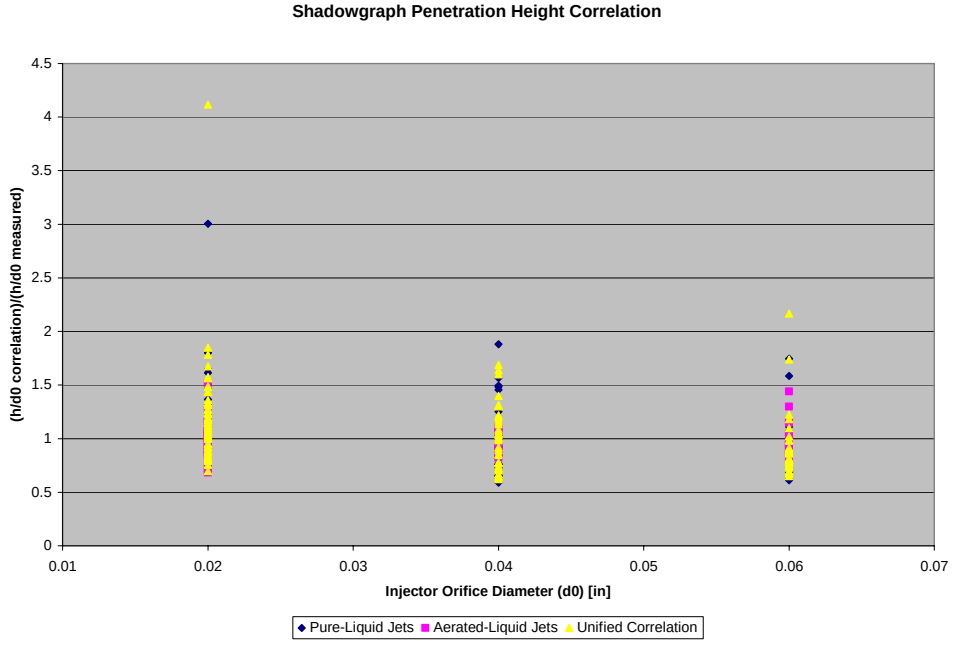

Figure 11: Spray penetration height correlation (h/d_0 correlation) derived from shadowgraphy, normalized by the measured penetration height (h/d_0 measured), graphed versus injector orifice diameter (d_0).

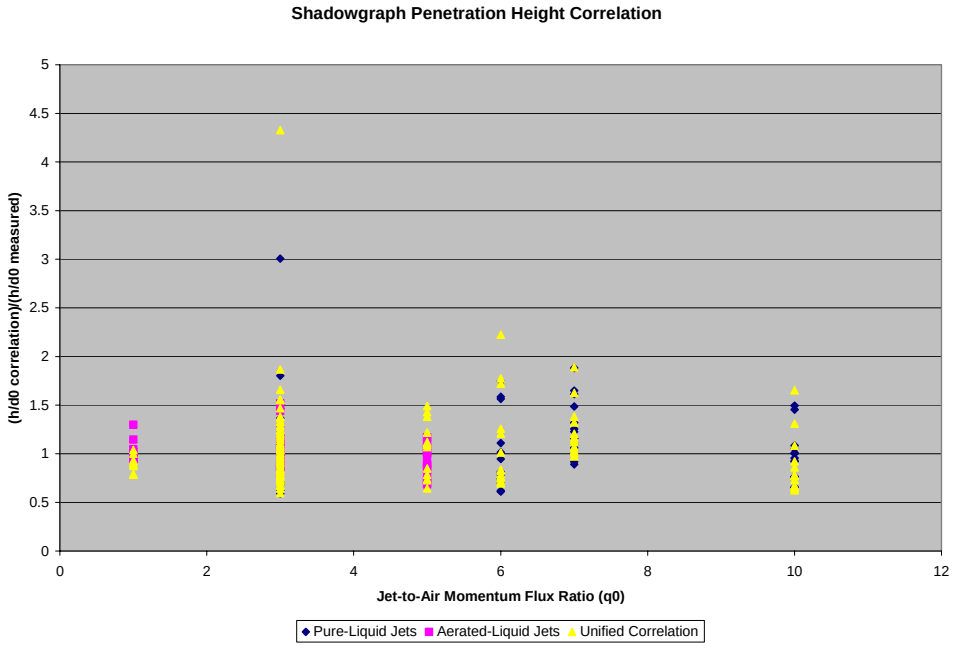

Figure 12: Spray penetration height correlation (h/d_0 correlation) derived from shadowgraphy, normalized by the measured penetration height (h/d_0 measured), graphed versus jet-to-air momentum flux ratio (q_0).

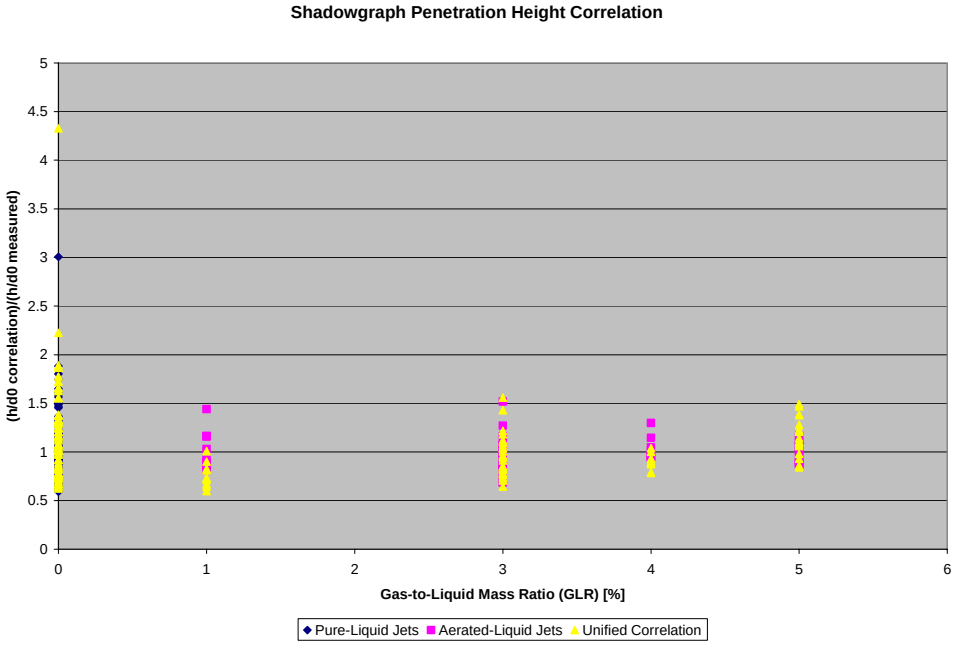

Figure 13: Spray penetration height correlation (h/d_0 correlation) derived from shadowgraphy, normalized by the measured penetration height (h/d_0 measured), graphed versus gas-to-liquid ratio (GLR).

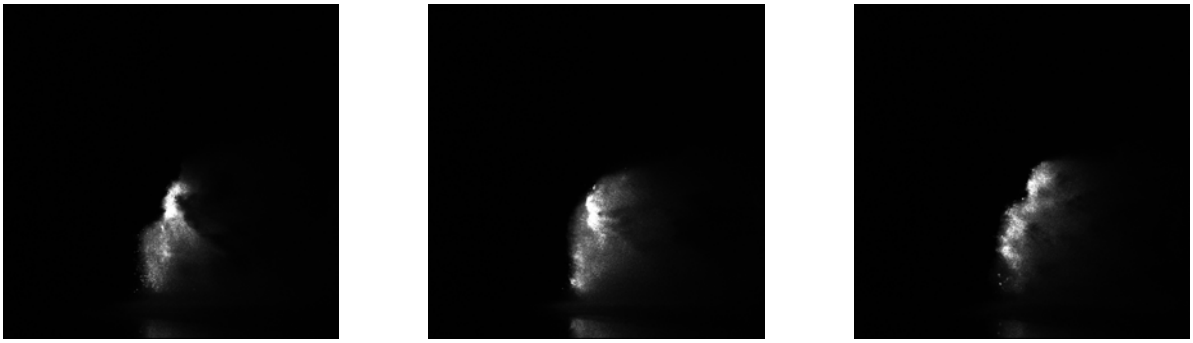

Figure 14: Consecutive laser sheet illumination images (unaltered). For these test conditions, θ=90°, d_0=0.060", q_0=3, GLR=0%. Images taken at axial location of x=0.2". Flow is out of the page.

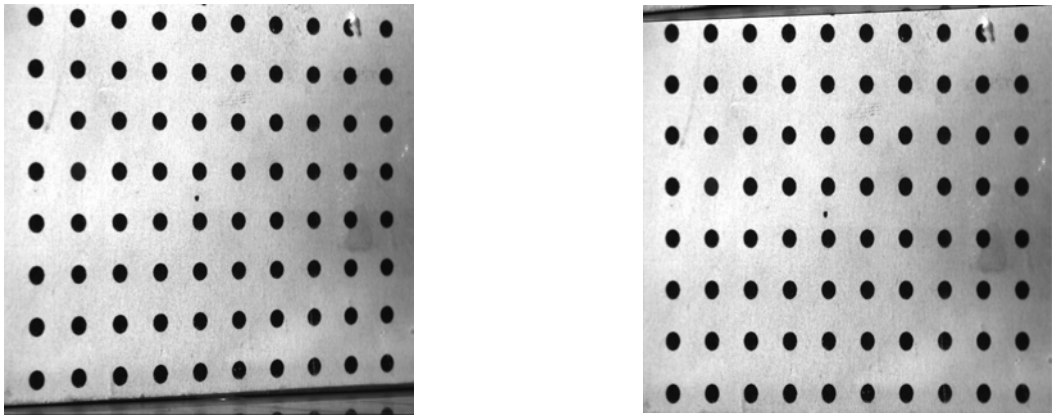

Original Dotcard Image | Unskewed Dotcard Image

Original (Averaged) Spray Plume Image | Unskewed Spray Plume Image

Figure 15: Comparison of original (skewed) laser sheet illumination images to unskewed images. For these test conditions, θ=90°, d_0=0.060", q_0=3, GLR=0%. Images of the spray plume taken at axial location of x=0.2". (Note that the spray plume images have been zoomed 4x to focus on the spray plume itself.) Flow is out of the page.

Grayscale Image Black and White Image

Figure 16: Comparison of grayscale laser sheet illumination image to black and white image. For these test conditions, θ=90°, d_0=0.060", q_0=3, GLR=0%. Images taken at axial location of x=0.2". Flow is out of the page.

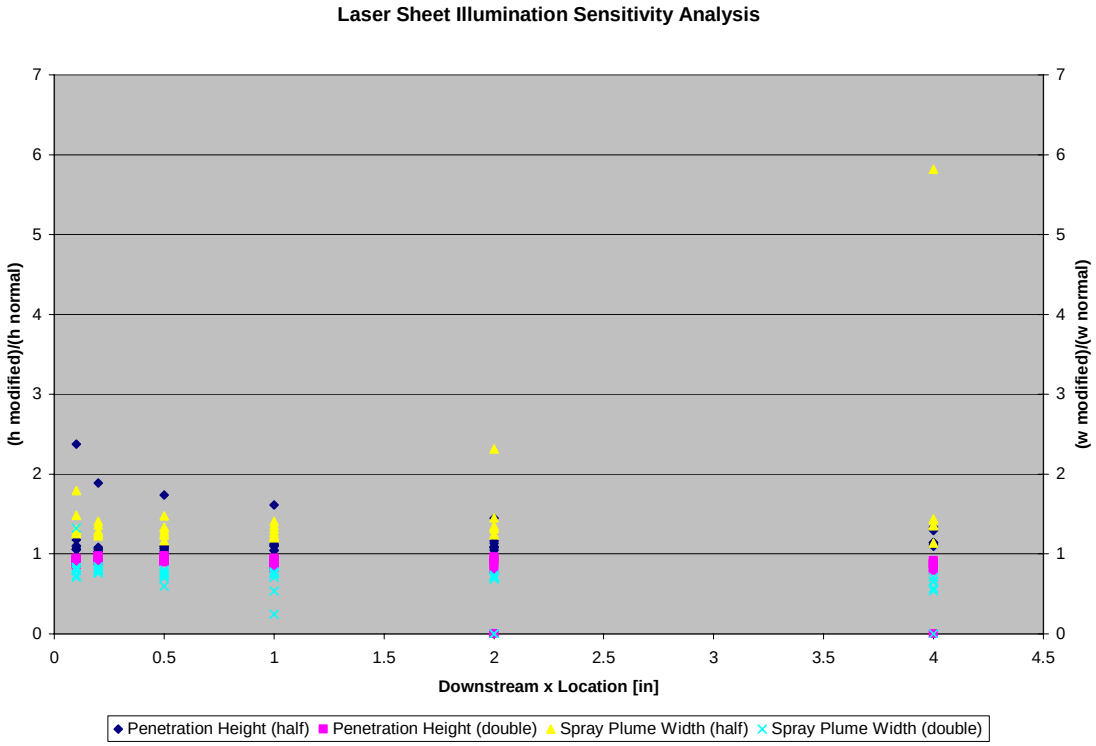

Figure 17: Sensitivity analysis showing the effects of increasing or decreasing the chosen intensity value for converting grayscale images to black and white images. The vertical axes show the new measured penetration height (both at half intensity and double intensity), normalized by the original measured penetration height, and the new measured spray plume width (both at half and double intensity), normalized by the original spray plume width.

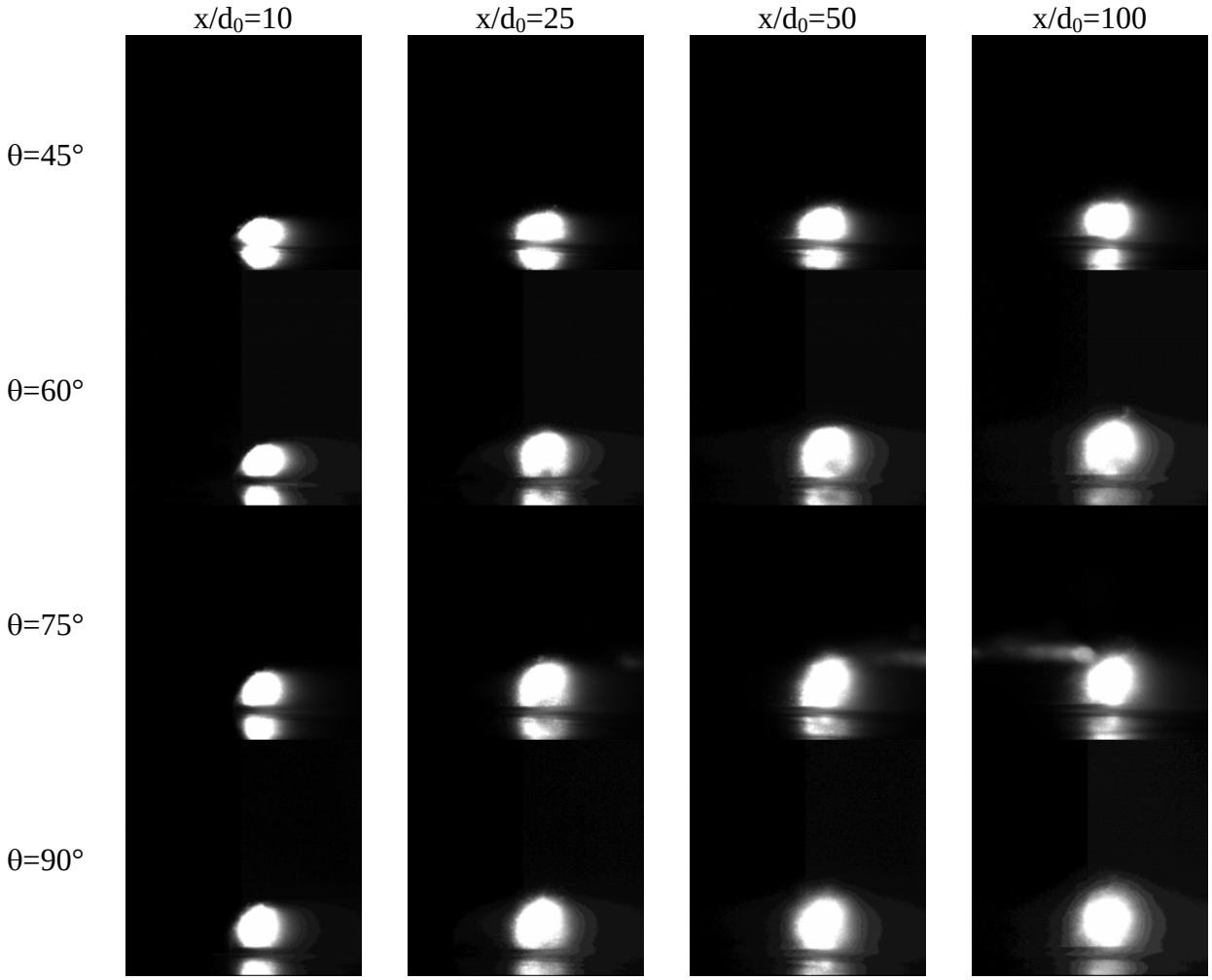

Figure 18: Laser sheet illumination imagery comparison of injection angles (θ). For these test conditions, d_0=0.020", q_0=3, and GLR=0%. (Contrast enhanced to show detail.) Flow is out of the page.

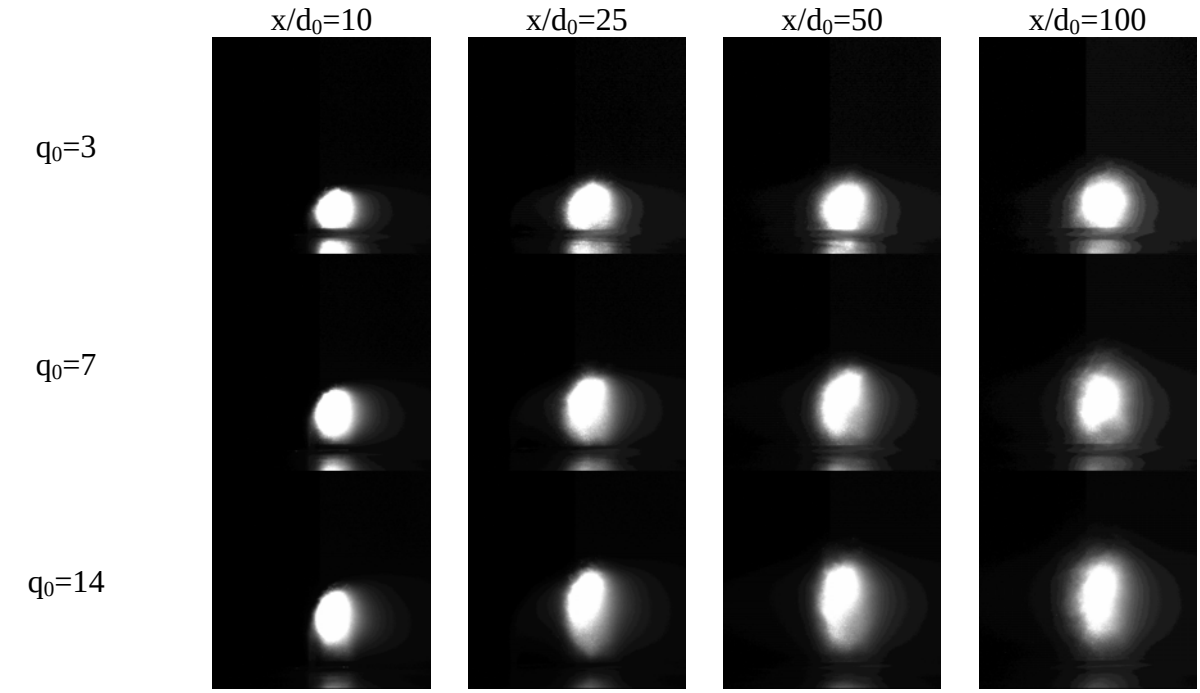

Figure 19: Laser sheet illumination imagery comparison of the effect of increasing jet-to-air momentum flux ratio (q_0). For these test conditions, θ=90°, d_0=0.020", and GLR=0%. (Contrast enhanced to show detail.) Flow is out of the page.

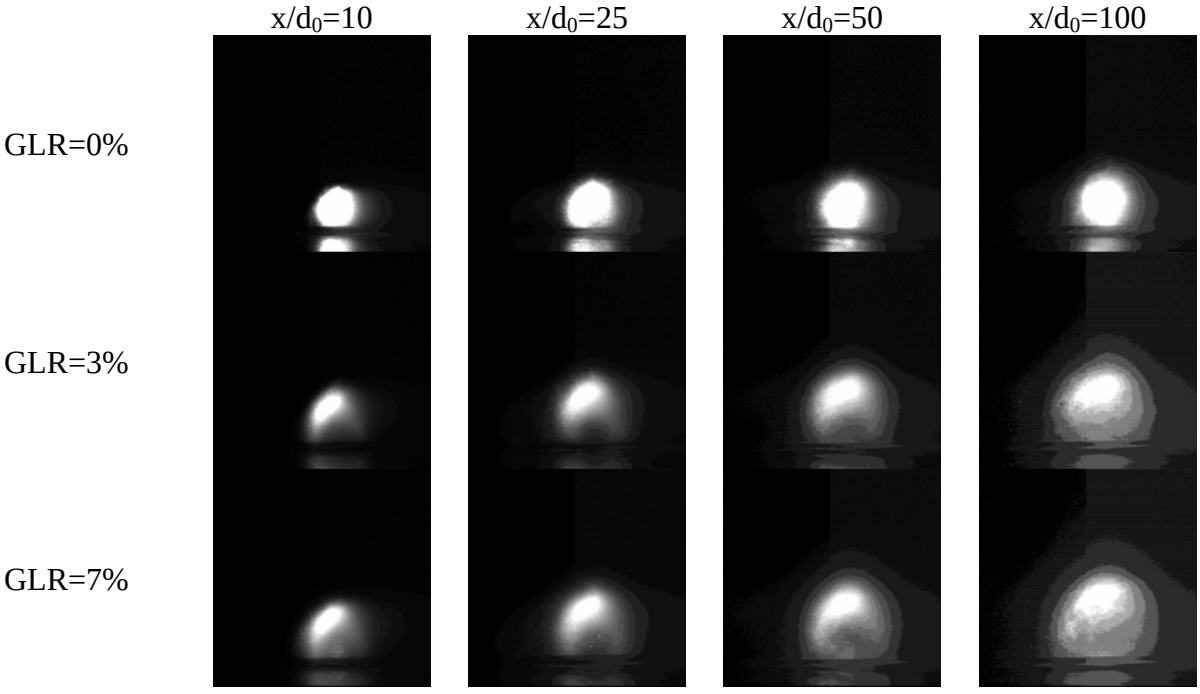

Figure 20: Laser sheet illumination imagery comparison of the effect of increasing gas-to-liquid ratio (GLR). For these test conditions, θ=90°, d_0=0.020", and q_0=3. (Contrast enhanced to show detail.) Flow is out of the page.

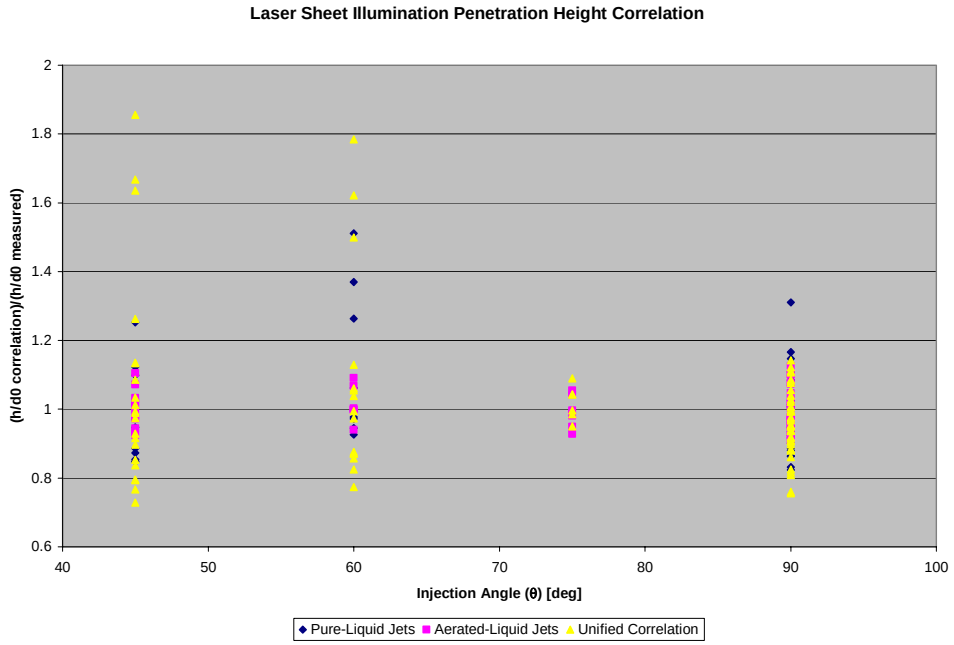

Figure 21: Spray penetration height correlations for pure- and aerated-liquid jets (h/d_0 correlation) derived from laser sheet illumination, normalized by the measured penetration height (h/d_0 measured), graphed versus injection angle (θ).

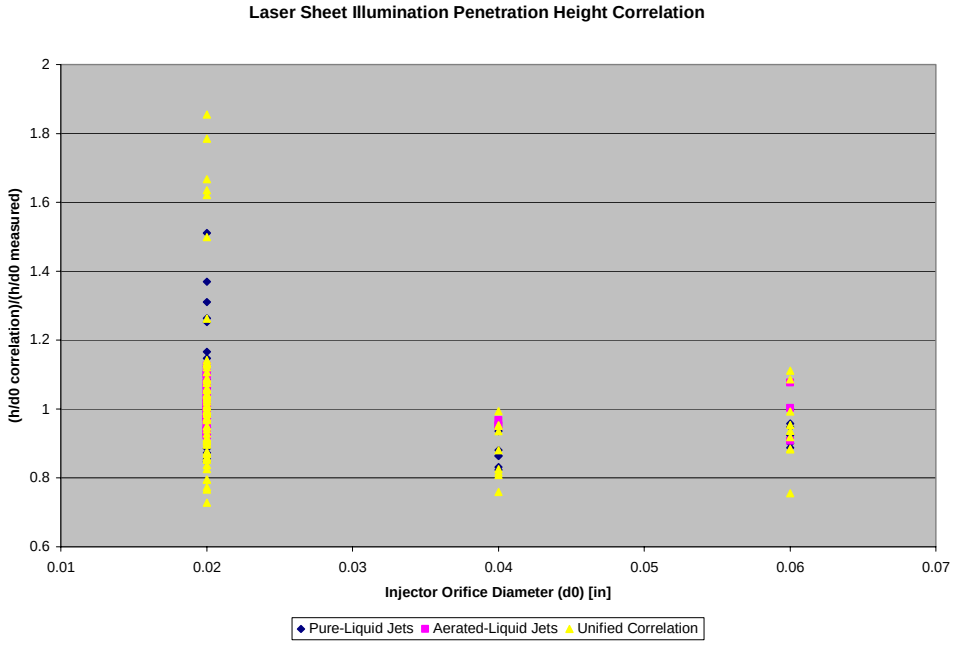

Figure 22: Spray penetration height correlations for pure- and aerated-liquid jets (h/d_0 correlation) derived from laser sheet illumination, normalized by the measured penetration height (h/d_0 measured), graphed versus injector orifice diameter (d_0).

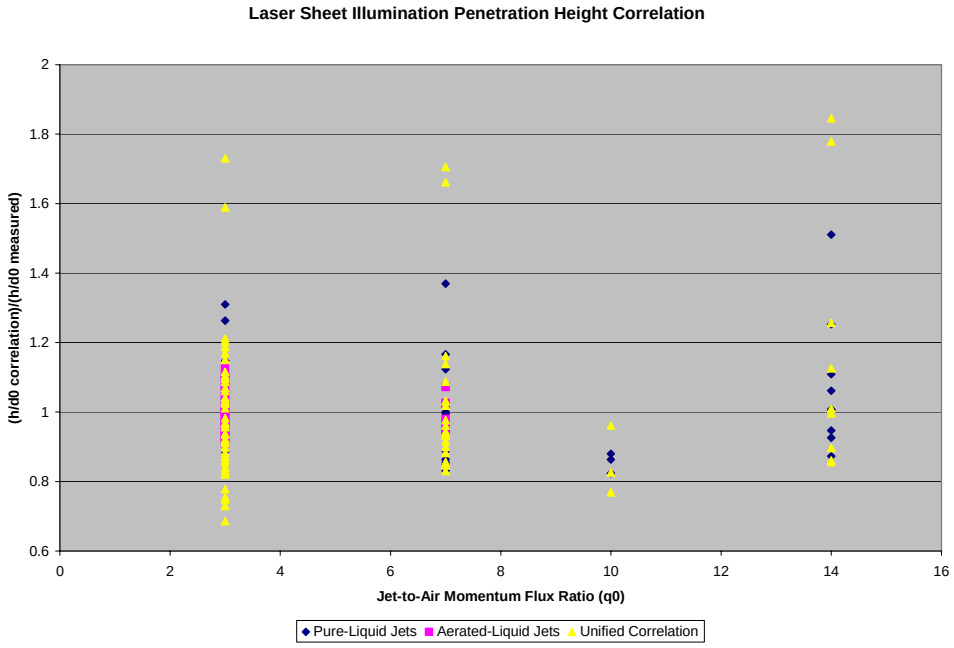

Figure 23: Spray penetration height correlations for pure- and aerated-liquid jets (h/d_0 correlation) derived from laser sheet illumination, normalized by the measured penetration height (h/d_0 measured), graphed versus jet-to-air momentum flux ratio (q_0).

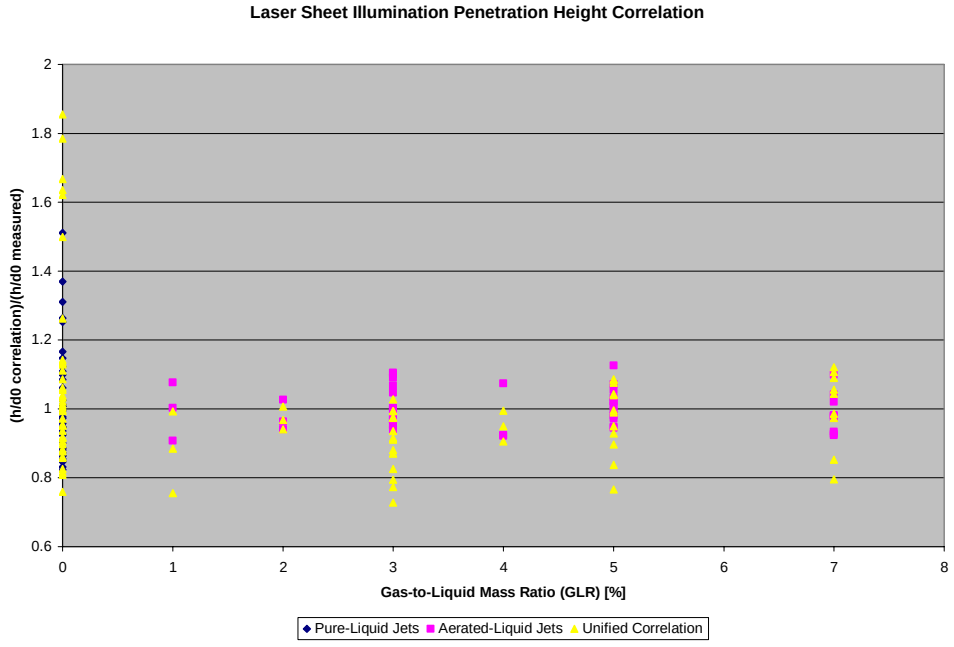

Figure 24: Spray penetration height correlation for pure- and aerated-liquid jets (h/d_0 correlation) derived from laser sheet illumination, normalized by the measured penetration height (h/d_0 measured), graphed versus gas-to-liquid mass ratio (GLR).

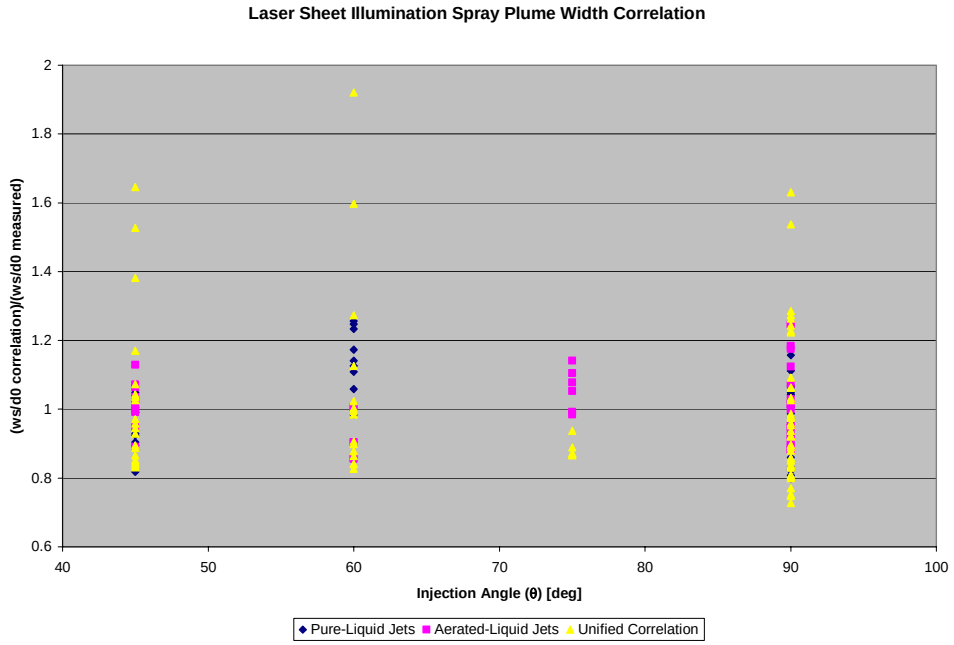

Figure 25: Spray plume width correlation for pure- and aerated-liquid jets (w_s/d_0 correlation) derived from laser sheet illumination, normalized by the measured spray plume width (w_s/d_0 measured), graphed versus injection angle (θ).

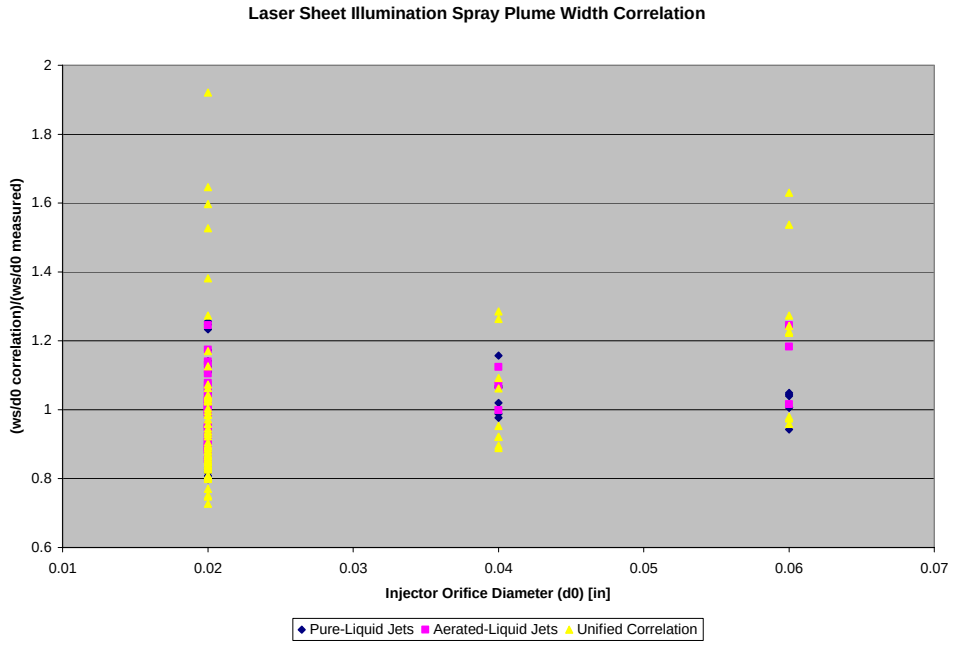

Figure 26: Spray plume width correlation for pure- and aerated-liquid jets (w_s/d_0 correlation) derived from laser sheet illumination, normalized by the measured spray plume width (w_s/d_0 measured), graphed versus injector orifice diameter (d_0).

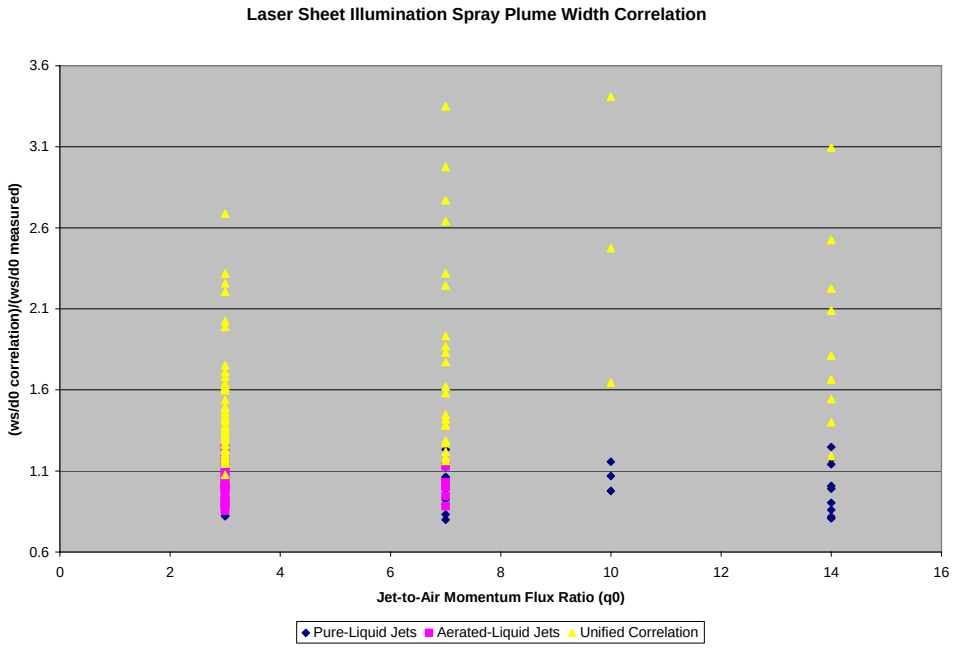

Figure 27: Spray plume width correlation for pure- and aerated-liquid jets (w_s/d_0 correlation) derived from laser sheet illumination, normalized by the measured spray plume width (w_s/d_0 measured), graphed versus jet-to-air momentum flux ratio (q_0).

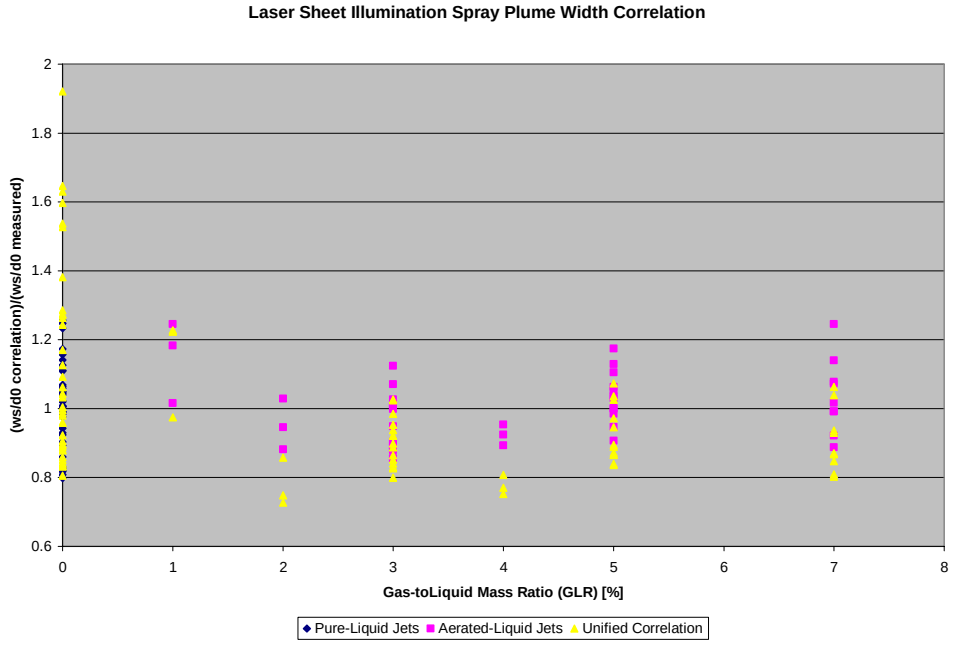

Figure 28: Spray penetration height and plume width correlations for pure- and aerated-liquid jets (h/d_0 correlation, w_s/d_0 correlation, respectively), normalized by the measured penetration height and plume width (h/d_0 measured, w_s/d_0 measured, respectively), graphed versus gas-to-liquid mass ratio (GLR).

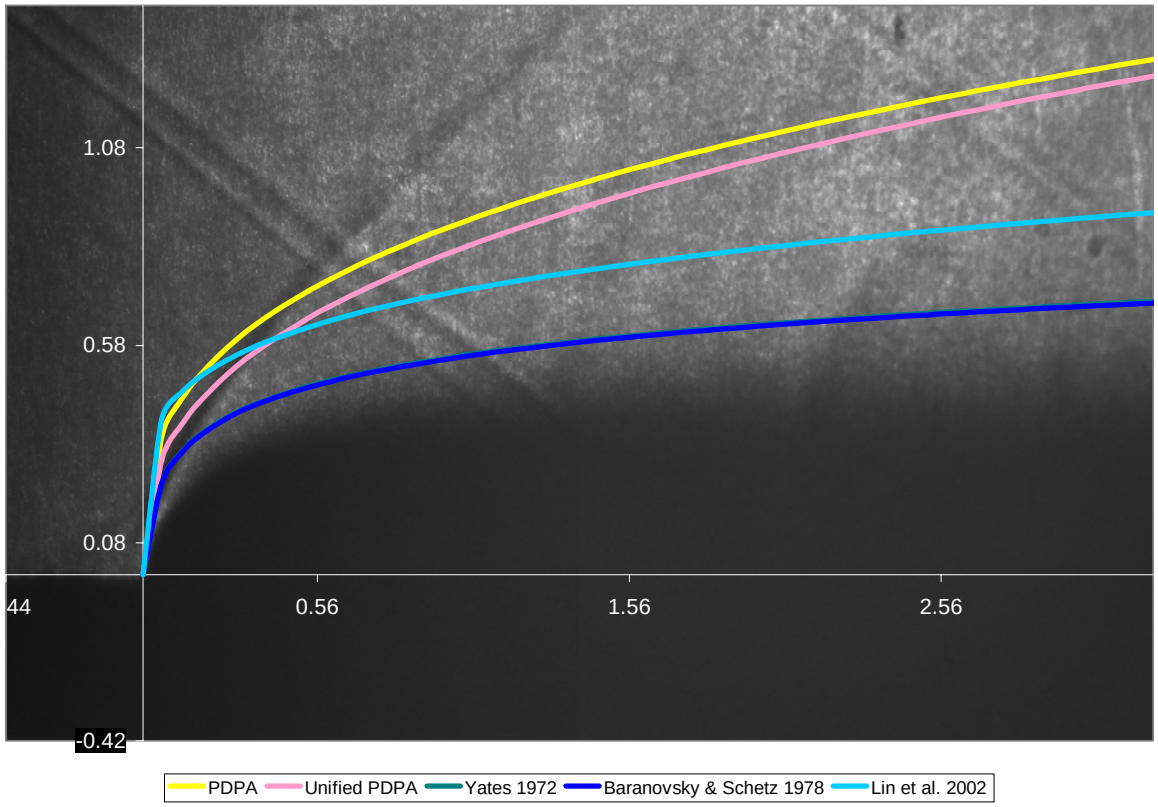

Figure 29: Comparison of historical correlations to current PDPA-derived correlations. For this test condition, θ=90°, d_0=0.060", q_0=3, and GLR=0%. (Note that the Yates 1972 and the Baranovsky & Schetz 1978 correlations align exactly on this graph.)

a)

b)

c)*

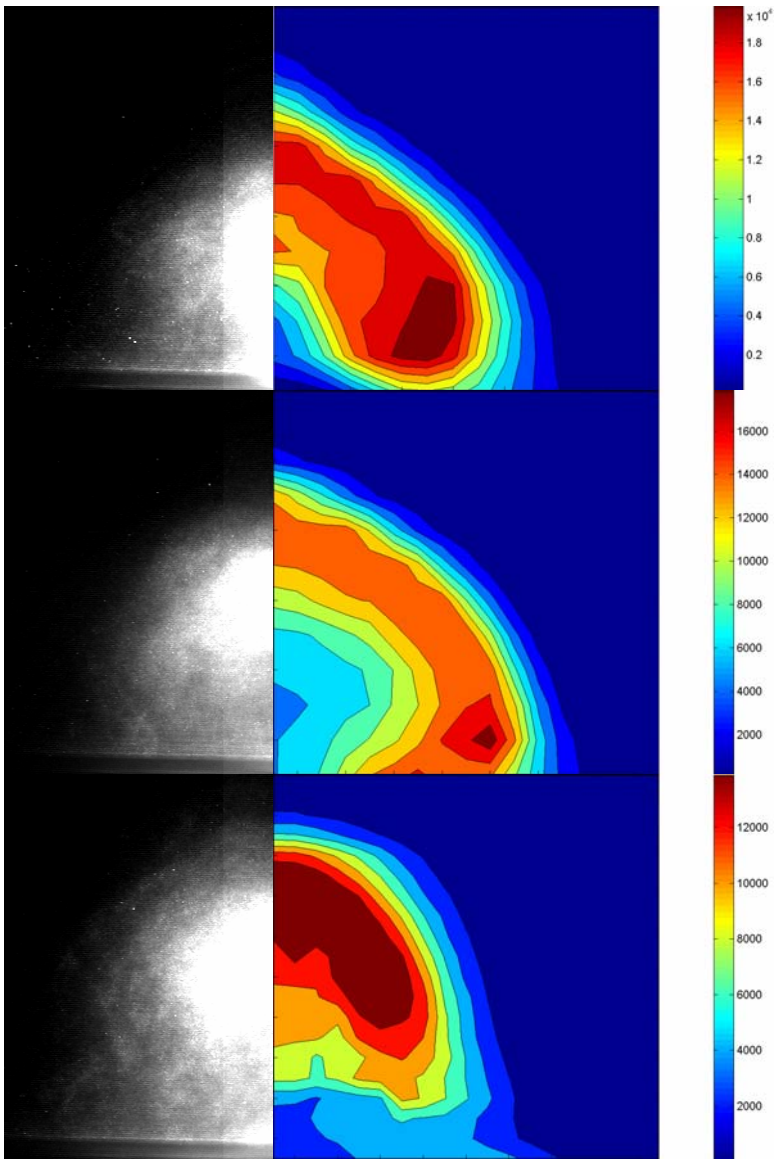

Figure 30: Comparison of laser sheet illumination imagery to phase Doppler particle analyzer data. The test conditions for each of these plots are as follows: a) θ=45°, d_0=0.020", q_0=3, GLR=7% , b) θ=45°, d_0=0.020", q_0=7, GLR=5%, c) θ=90°, d_0=0.020", q_0=7, GLR=2%. (Contrast enhanced on laser sheet images to show detail.) (Spray plumes shown half-width.) *Denotes PDPA measurements taken by Lin et al.[12] included for completeness.

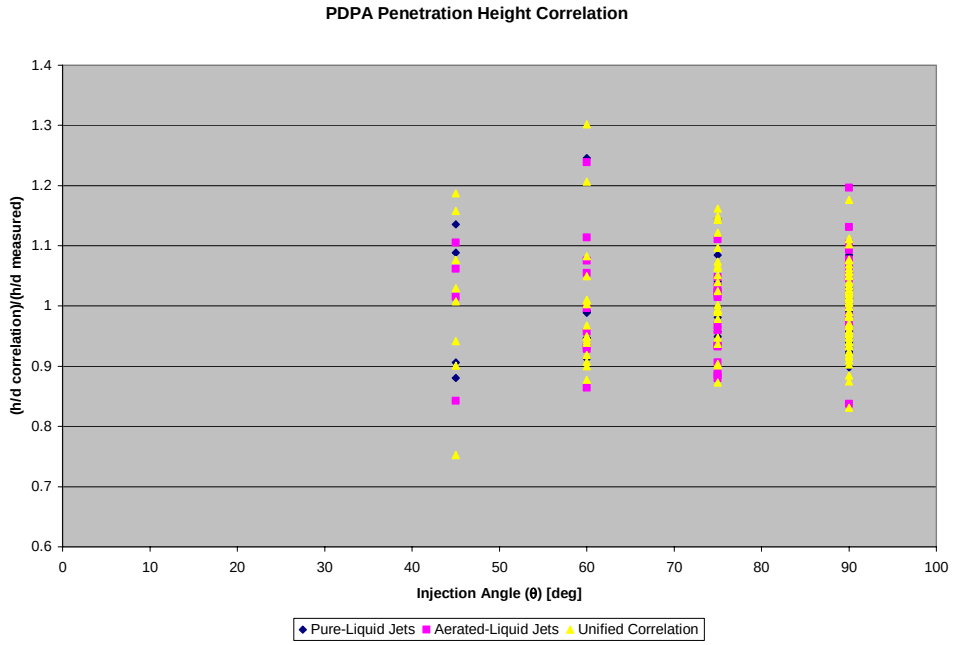

Figure 31: Spray penetration height correlations for pure-and aerated-liquid jets (h/d_0 correlation), normalized by the measured penetration height (h/d_0 measured), graphed versus injection angle (θ).

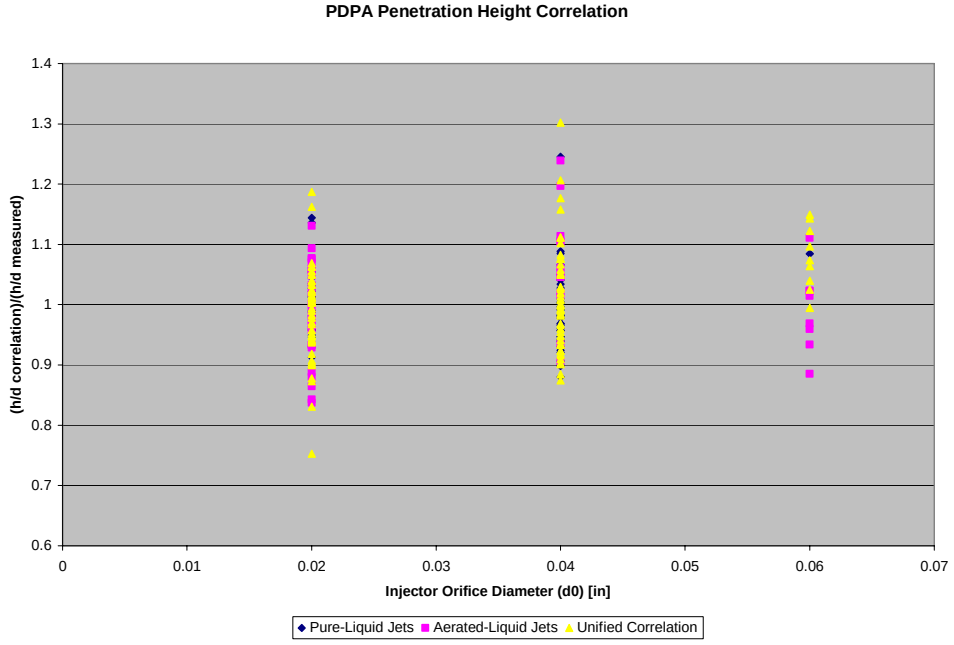

Figure 32: Spray penetration height correlations for pure- and aerated-liquid jets (h/d_0 correlation), normalized by the measured penetration height (h/d_0 measured), graphed versus injector orifice diameter (d_0).

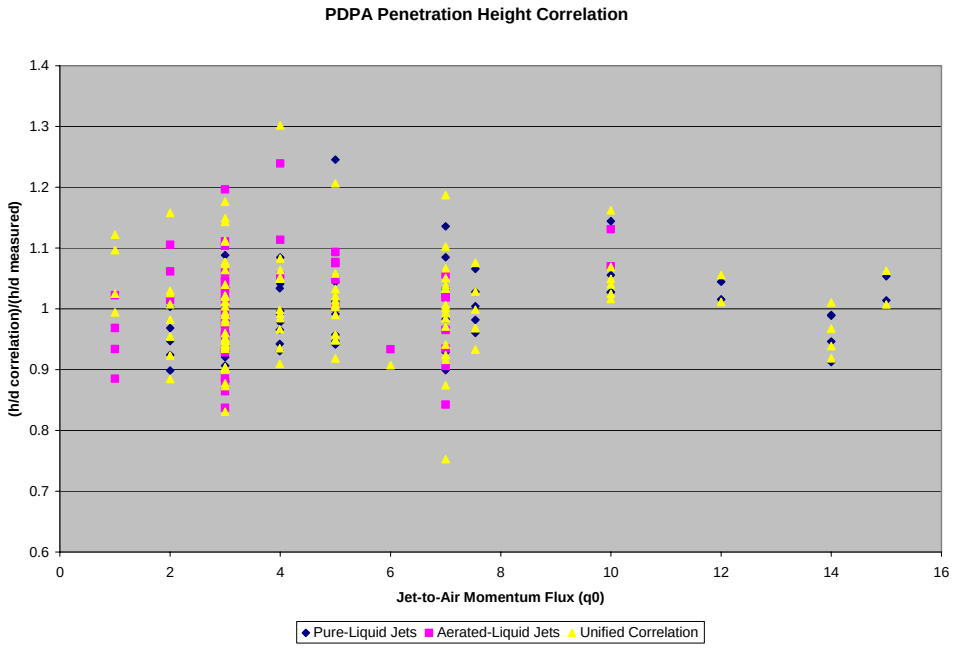

Figure 33: Spray penetration height correlations for pure- and aerated-liquid jets (h/d_0 correlation), normalized by the measured penetration height (h/d_0 measured), graphed versus jet-to-air momentum flux ratio (q_0).

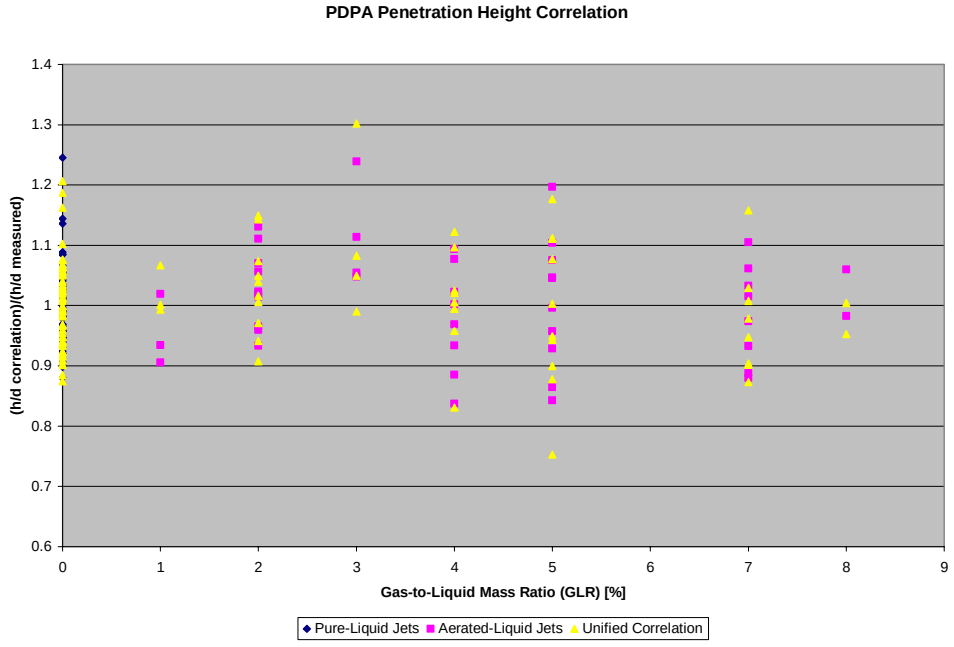

Figure 34: Spray penetration height correlations for pure- and aerated-liquid jets (h/d_0 correlation), normalized by the measured penetration height (h/d_0 measured), graphed versus gas-to-liquid mass ratio (GLR).

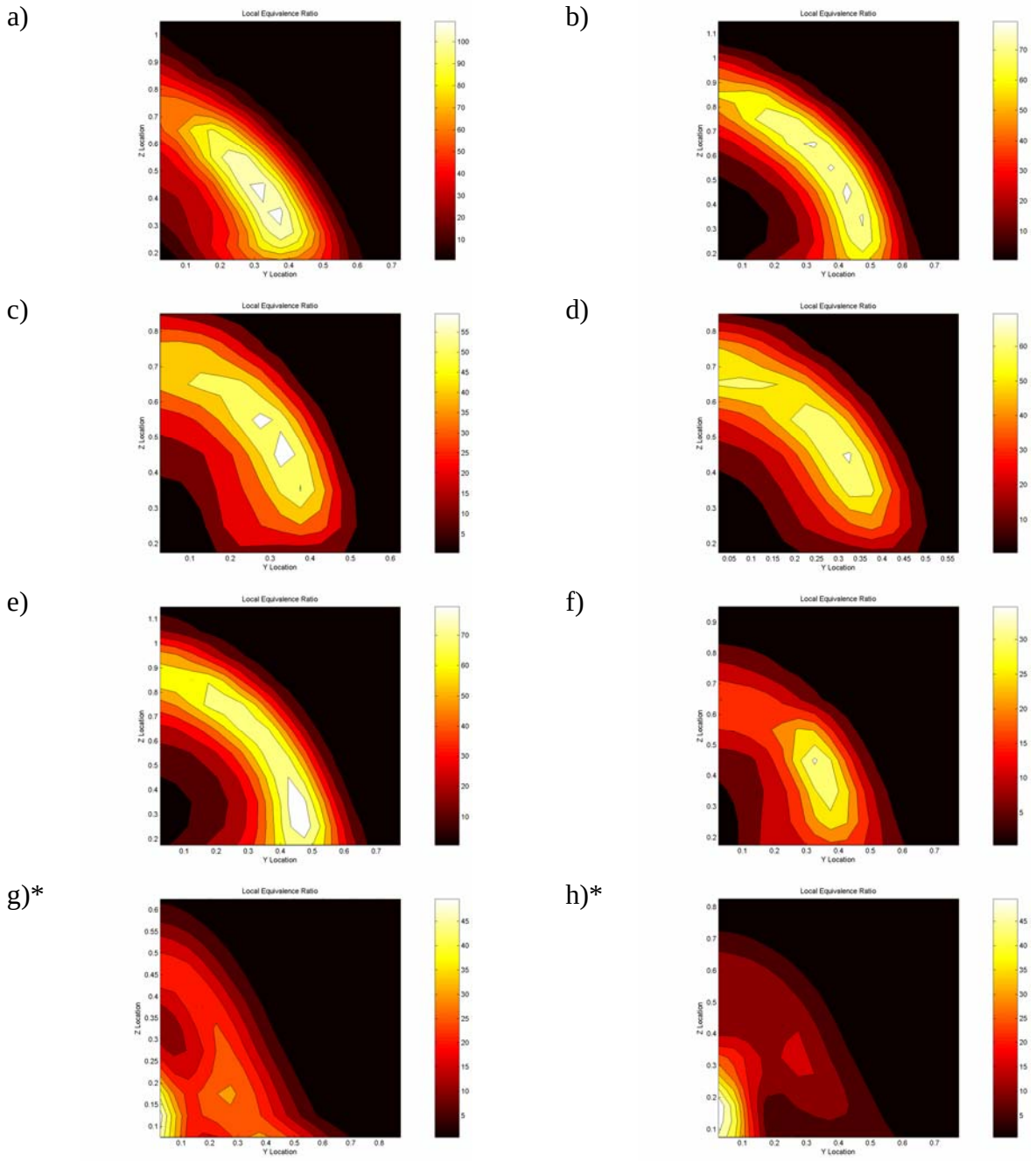

Figure 35: Half-plume plots of local equivalence ratios derived from PDPA measurements. The test conditions for each of these plots are as follows: a) θ=45°, d_0=0.020". q_0=3, GLR=7%, b) θ=45°, d_0=0.020". q_0=7, GLR=5%, c) θ=60°, d_0=0.020". q_0=5, GLR=5%, d) θ=60°, d_0=0.020". q_0=6, GLR=2%, e) θ=75°, d_0=0.020". q_0=5, GLR=3%, f) θ=75°, d_0=0.020". q_0=10, GLR=0%, g) θ=90°, d_0=0.020". q_0=3, GLR=0%, h) θ=90°, d_0=0.020". q_0=3, GLR=8%. (Plumes are shown half-width.) *Denotes PDPA measurements taken by Lin et al.[12] included for completeness.

APPENDIX A

Shadowgraph Intensity Profile Script

```
cd c:\thesis\Shadowgraph\Day1

DNames = dir;

MeanMatrix = double(zeros(length(DNames)-2,2));

for i = 3:length(DNames)
   eval(['cd c:\thesis\Shadowgraph\Day1\',DNames(i).name]);
   eval(['I = imread('',DNames(i).name,'sg.tif');']);
   eval(['I',DNames(i).name,' = uint16(zeros(1023,5));']);
   for j=1:1023
      I(1,:) = [];
   end
   A = uint16(zeros(274,1500));
   for j=1:274
      for k=549:2048
         A(j,k-548) = I(j,k);
      end
   end
   M = mean2(A);
   MeanMatrix(i-2,1) = str2num(DNames(i).name);
   MeanMatrix(i-2,2) = M;
   eval(['I',DNames(i).name,'(:,1) = I(:,319);']);
   eval(['I',DNames(i).name,'(:,2) = I(:,374);']);
   eval(['I',DNames(i).name,'(:,3) = I(:,538);']);
   eval(['I',DNames(i).name,'(:,4) = I(:,812);']);
   eval(['I',DNames(i).name,'(:,5) = I(:,1361);']);
   eval(['I',DNames(i).name,'(:,6) = I(:,319)/uint16(round(M*65535));']);
   eval(['I',DNames(i).name,'(:,7) = I(:,374)/uint16(round(M*65535));']);
   eval(['I',DNames(i).name,'(:,8) = I(:,538)/uint16(round(M*65535));']);
   eval(['I',DNames(i).name,'(:,9) = I(:,812)/uint16(round(M*65535));']);
   eval(['I',DNames(i).name,'(:,10) = I(:,1361)/uint16(round(M*65535));']);
   eval(['dlmwrite("c:\thesis\Shadowgraph\',DNames(i).name,'.txt", I',DNames(i).name,',
"delimiter", "\t", "precision", 8);']);
   eval(['clear I',DNames(i).name,';']);
end

dlmwrite('c:\thesis\Shadowgraph\Day1Means.txt', MeanMatrix, 'delimiter', '\t', 'precision', 8);

clear all;

cd c:\thesis\Shadowgraph\Day2
```

```
DNames = dir;

MeanMatrix = double(zeros(length(DNames)-2,2));

for i = 3:length(DNames)
   eval(['cd c:\thesis\Shadowgraph\Day2\',DNames(i).name]);
   eval(['I = imread('',DNames(i).name,'sg.tif');']);
   eval(['I',DNames(i).name,' = uint16(zeros(1023,5));']);
   for j=1:1023
      I(1,:) = [];
   end
   A = uint16(zeros(274,1500));
   for j=1:274
      for k=549:2048
         A(j,k-548) = I(j,k);
      end
   end
   M = mean2(A);
   MeanMatrix(i-2,1) = str2num(DNames(i).name);
   MeanMatrix(i-2,2) = M;
   eval(['I',DNames(i).name,'(:,1) = I(:,319);']);
   eval(['I',DNames(i).name,'(:,2) = I(:,374);']);
   eval(['I',DNames(i).name,'(:,3) = I(:,538);']);
   eval(['I',DNames(i).name,'(:,4) = I(:,812);']);
   eval(['I',DNames(i).name,'(:,5) = I(:,1361);']);
   eval(['I',DNames(i).name,'(:,6) = I(:,319)/M;']);
   eval(['I',DNames(i).name,'(:,7) = I(:,374)/M;']);
   eval(['I',DNames(i).name,'(:,8) = I(:,538)/M;']);
   eval(['I',DNames(i).name,'(:,9) = I(:,812)/M;']);
   eval(['I',DNames(i).name,'(:,10) = I(:,1361)/M;']);
   eval(['dlmwrite("c:\thesis\Shadowgraph\',DNames(i).name,'.txt", I',DNames(i).name,',
"delimiter", "\t", "precision", 8);']);
   eval(['clear I',DNames(i).name,';']);
end

dlmwrite('c:\thesis\Shadowgraph\Day2Means.txt', MeanMatrix, 'delimiter', '\t', 'precision', 8);

clear all;
```

8bit Image Averaging Script

```
ImgMatrix = uint8(zeros(1024,1024,50));

   FileNames = dir('*.tif');

   for i=1:6
      for j=((i-1)*50)+1:i*50
         ImgMatrix(:,:,j-((i-1)*50)) = imread(FileNames(j).name);
      end

      AvgImg = uint8(mean(ImgMatrix,3));
      eval(['imwrite(AvgImg,"average0',num2str(i),'.tif","TIFF")']);
   end
clear all;
```

16bit Image Averaging Script

```
ImgMatrix = uint16(zeros(1024,1024,50));

   FileNames = dir('*.tif');

   for i=1:6
      for j=((i-1)*50)+1:i*50
         ImgMatrix(:,:,j-((i-1)*50)) = imread(FileNames(j).name);
      end

      AvgImg = uint16(mean(ImgMatrix,3));
      eval(['imwrite(AvgImg,"average0',num2str(i),'.tif","TIFF")']);
   end
clear all;
```

Image Unskewing Script

```
DirNames = dir;
DNLength = length(DirNames);

T = maketform('projective',[79 31; 955 62; 83 937; 957 895],[79 31; 955 31; 83 937; 957 937]);
R = makeresampler('cubic','circular');

for i=3:DNLength
   eval(['cd c:\thesis\lasersheet\16bit\',DirNames(i).name,'\']);
   for j=1:6
      eval(['I',num2str(j),' = imread("',DirNames(i).name,'avg0',num2str(j),'.tif");']);
      eval(['K',num2str(j),' = imtransform(I',num2str(j),',T,R,"Size",[1024 1024],"XYScale",1);']);
      eval(['imwrite(K',num2str(j),',"',DirNames(i).name,'avg0',num2str(j),'unskew.tif","TIFF");']);
   end
end
```

Grayscale to Black-and-White Matlab Script

```
clear all;
clc;

cd c:\thesis\lasersheet\8bit\

% Read the names of the directories and store them in a matrix
DNames = dir;

% Remove the first two entries from the matrix, which are by default
% the values "." and ".."
DNames(1) = []; DNames(1) = [];

% Begin recursing through the directories and reading in the images
for i = 1:length(DNames)
   eval(['cd c:\thesis\lasersheet\8bit\',DNames(i).name,'\']);
   for j=1:6
      % Read in each of the 6 averaged images, one at a time
      eval(['I = imread("',DNames(i).name,'avg0',num2str(j),'unskew.tif");']);
      % Convert the image to black and white
      BW = im2bw(I,0.025);
      % Write the black and white image to a TIF file
      eval(['imwrite(BW, "',DNames(i).name,'avg0',num2str(j),'BW.tif", "TIFF");']);
   end
end

clear all;
clc;

cd c:\thesis\lasersheet\16bit\

% Read the names of the directories and store them in a matrix
DNames = dir;

% Remove the first two entries from the matrix, which are by default
% the values "." and ".."
DNames(1) = []; DNames(1) = [];

% Begin recursing through the directories and reading in the images
for i = 1:length(DNames)
   eval(['cd c:\thesis\lasersheet\16bit\',DNames(i).name,'\']);
   for j=1:6
      % Read in each of the 6 averaged images, one at a time
      eval(['I = imread("',DNames(i).name,'avg0',num2str(j),'unskew.tif");']);
      % Convert the image to black and white
      BW = im2bw(I,0.025);
```

```
      % Write the black and white image to a TIF file
      eval(['imwrite(BW, '',DNames(i).name,'avg0',num2str(j),'BW.tif'', ''TIFF'');']);
   end
end
```

PDPA Equivalence Ratio Script

```
%This file reads in tab delimited text files created from Excel
%spreadsheets.  The first file read in is a file called 'List.txt' which
%lists all of the conditions being read in as well as the global
%equivalence ratio for each condition.

%The second file read in is of the naming convention AADDQQGGVF.txt, where
%AA=injection angle in degrees, DD=orifice diameter in thousandths of an
%inch, QQ=jet-to-air momentum flux, and GG=gas-to-liquid ratio in
%percentage.  This file contains the volume flux measurements made by the
%PDPA system in cubic centimeters per square centimeter per second.

%The third file read in is a two column file listing the y-locations (in
%inches) of each measurement in the first column and the z-locations (in
%inches) of each measurement in the second column.  This file is of the
%naming convention AADDQQGGArea.txt.

%The fourth file lists the particle concentrations at each location.  Naming
%convention is AADDQQGGPC.txt.

%Clears all variables.
clear all;

%Creates an array containing the list of these files in the directory.
Names = dlmread('List.txt');

%Begins recursing through the files in the directory.
for k=1:length(Names)

%Reads the first files in and stores them as arrays.
   eval(['VF = dlmread('',num2str(Names(k,1)),'VF.txt'');']);
   eval(['ATxt = dlmread('',num2str(Names(k,1)),'Area.txt'');']);
   eval(['PC = dlmread('',num2str(Names(k,1)),'PC.txt'');']);

%Creates a contour plot of the particle concentration at each location and
%saves it as a TIF file.
   [c,h] = contourf(PC');
   colormap default;
   axis square tight;
   colorbar;
   eval(['saveas(h,'',num2str(Names(k,1)),'PC.tif'',''tif'');']);
```

```
   close
   clear h; clear c;

%Determines the size of the volume flux array.
   d = size(VF);

%Begins recursing through the arrays.
   for i=1:d(1)-1
      for j=1:d(2)-1

%Takes the average of the volume flux values creating a four point box
%throughout the array. [cc/(cm^2*s)]
         VFavg(i,j) = (VF(i,j)+VF(i+1,j)+VF(i,j+1)+VF(i+1,j+1))/4;

%Calculates the equivalence ratio based on liquid mass flux, air mass flux,
%and a stoichiometric fuel/air ratio of 0.06719, then normalizes it by the
%global equivalence ratio for each condition.
         EqRatio(i,j) = ((VFavg(i,j)/22.875)/0.06719)/Names(k,2);

%Creates X matrix of the x coordinates.
         X(1,j) = (ATxt(j+1,1)+ATxt(j,1))/2;
      end

%Creates Y matrix of the y coordinates.
      Y(1,i) = (ATxt(i+1,2)+ATxt(i,2))/2;
   end

%Creates a contour plot of the equivalence ratio values and saves it as a
%TIF file.  It was discovered that the axes were reversed in the matrix, thus
%the transpose of the matrix is plotted and the axes are switched.
   [c,h] = contourf(Y,X,EqRatio');
   colormap hot;
   axis square tight;
   colorbar;
   xlabel('Y Location');
   ylabel('Z Location');
   title('Local Equivalence Ratio');
   eval(['saveas(h,'',num2str(Names(k,1)),'ER.tif","tif");']);
   close;
   clear h; clear c;

%Outputs a tab delimited text file containing the local equivalence ratios
%in the plume.

   eval(['dlmwrite('',num2str(Names(k,1)),'.txt",EqRatio,"\t");']);
   clear VF; clear EqRatio; clear ATxt; clear PC; clear VFavg;
```

```
    clear X; clear Y; clear d;
end
```

Particle Concentration and SMD Averaging Script

```
%This file reads in tab delimited text files created from Excel
%spreadsheets.  The first file read in is a file called 'List.txt' which
%lists all of the conditions being read in as well as the global
%equivalence ratio for each condition.

%The second file read in is of the naming convention AADDQQGGArea.txt, where
%AA=injection angle in degrees, DD=orifice diameter in thousandths of an
%inch, QQ=jet-to-air momentum flux, and GG=gas-to-liquid ratio in
%percentage.  This file contains is a two column file listing the
%y-locations (in inches) of each measurement in the first column and the
%z-locations (in inches) of each measurement in the second column.

%The third file read in has the Sauter Mean Diameter values.  This file is
%of the naming convention AADDQQGGSMD.txt.  SMD are given in units of
%micrometers.

%The fourth file lists the particle concentrations at each location.  Naming
%convention is AADDQQGGPC.txt.

%Clears all variables.
clear all;

%Creates an array containing the list of these files in the directory.
Names = dlmread('List.txt');

%Begins recursing through the files in the directory.
for k=1:length(Names)

%Reads the first files in and stores them as arrays.
   eval(['ATxt = dlmread('',num2str(Names(k,1)),'Area.txt'');']);
   eval(['SMD = dlmread('',num2str(Names(k,1)),'SMD.txt'');']);
   eval(['PC = dlmread('',num2str(Names(k,1)),'PC.txt'');']);

%Determines the size of the volume flux array.
   d = size(SMD);

%Begins recursing through the arrays.
   for i=1:d(1)-1
      for j=1:d(2)-1

%Takes the average of the SMD values and particle concentration values
%creating a four point box throughout the array. [cc/(cm^2*s)], [1/cc]
         SMDavg(i,j) = (SMD(i,j)+SMD(i+1,j)+SMD(i,j+1)+SMD(i+1,j+1))/4;
         PCavg(i,j) = (PC(i,j)+PC(i+1,j)+PC(i,j+1)+PC(i+1,j+1))/4;
```

```
%Creates X matrix of the x coordinates.
          X(1,j) = (ATxt(j+1,1)+ATxt(j,1))/2;
       end

%Creates Y matrix of the y coordinates.
       Y(1,i) = (ATxt(i+1,2)+ATxt(i,2))/2;
   end

%Creates a contour plot of the SMD average values and saves it as a
%TIF file.
   [c,h] = contourf(X,Y,SMDavg);
   colormap default;
   colorbar;
   axis equal;
   eval(['saveas(h,'',num2str(Names(k,1)),'SMD.tif','tif');']);

%Creates a contour plot of the particle concentration at each location and
%saves it as a TIF file.
   [c,h] = contourf(X,Y,PCavg);
   colormap default;
   colorbar;
   axis equal;
   eval(['saveas(h,'',num2str(Names(k,1)),'PC.tif','tif');']);

end
```

BIBLIOGRAPHY

1. Kanury, A. Murty, *Introduction to Combustion Phenomena.* New York: Gordon and Breach Publishers, 1995.
2. Gretzinger, J., Marshall, W. R., Jr., "Characteristics of Pneumatic Atomization," *Journal of American Institute of Chemical Engineers*, Vol. 7, No. 2, 1961, pp. 312-318.
3. Lefebvre, A. H., Wang, X. F., Martin, C. A., "Spray Characteristics of Aerated-Liquid Pressure Atomizers," *Journal of Propulsion and Power*, Vol. 4, No. 4, 1988, pp. 293-298.
4. Lin, K.-C., Kennedy, P. J., Jackson, T. A., "Structures of Internal Flow and The Corresponding Spray For Aerated-Liquid Injectors," AIAA Paper 2001-3569, July 2001.
5. Sabel'nikov, V. A., Korontsvit, Y. P., Schadow, K., Ivanov V. V., Voloschenko, O. V., Zosimov, S. A., "Investigation of Supersonic Combustion Enhancement Using Barbotage and Injectors With Noncircular Nozzles," AIAA Paper 98-1516, 1998.
6. Mathur, T., Lin, K.-C., Kennedy, P., Gruber, M., Donbar, J., Jackson T., Billig, F., "Liquid JP-7 Combustion in a Scramjet Combustor," AIAA Paper 2000-3581, July 2000.
7. Lin, K.-C., Kirkendall, K. A., Kennedy, P. J., Jackson, T. A., "Spray Structures of Aerated-Liquid Fuel Jets in Supersonic Crossflows," AIAA Paper 99-2374, June 1999.
8. Lin, K.-C., Kennedy P. J., Jackson, T. A., "Spray Penetration Heights of Angled-Injected Aerated-Liquid Jets in Supersonic Crossflows," AIAA Paper 2000-0194, January 2000.
9. Lin, K.-C., Kennedy, P. J., Jackson, T. A., "Spray Structures of Aerated-Liquid Jets in Subsonic Crossflows," AIAA Paper 2001-0330, January 2001.
10. Lin, K.-C., Kennedy, P. J., Jackson, T. A., "Penetration Heights of Liquid Jets in High-Speed Crossflows," AIAA Paper 2002-0873, January 2002.
11. Lin, K.-C., Kennedy, P. J., Jackson, T. A., "Structures of Aerated-Liquid Jets in High-Speed Crossflows," AIAA Paper 2002-3178, June 2002.
12. Lin, K.-C., Kennedy, P. J., Jackson, T. A., "Structures of Water Jets in a Mach 1.94 Supersonic Crossflow," AIAA Paper 2004-0971, January 2004.
13. Fry, R. S, Edwards, T., "JP-7," CPIA/M6, Unit No. 8, September 2002.
14. Sallam, K. A., Aalburg, C., Faeth, G. M., *Dynamics of Breakup of Aerated-Liquid Jets in Supersonic Crossflows: Final Report, 1 August 2002 – 31 December 2003*, Award Ref. Nos. T002-32-16-006 and T003-26-01-001, Ann Arbor, Michigan: University of Michigan, 15 February 2004 (GDL/GMF-04-01).
15. Gruber, M., Baurle, R., Mathur, T., and Hsu, K., "Fundamental Studies of Cavity-Based Flameholder Concepts for Supersonic Combustors," AIAA Paper 99-2248, June, 1999.
16. Gruber, M. R., Nejad, A. S., "Development of a Large-Scale Supersonic Combustion Research Facility," AIAA Paper 94-0544, January, 1994

Vita

First Lieutenant Dion R. Dixon graduated from Lake Braddock Secondary School in Burke, Virginia in 1997. He entered undergraduate studies at the Pennsylvania State University, University Park, Pennsylvania, where he graduated with a Bachelor of Science degree in Aerospace Engineering in May 2002. He was commissioned through the Air Force Reserve Officer Training Corps Detachment 720.

His first assignment was at Wright-Patterson AFB as a High Speed Systems Developmental Engineer in the Propulsion Directorate of the Air Force Research Laboratory in June 2002. While assigned to AFRL, he enrolled as a part-time student at the Air Force Institute of Technology in January 2003 and was accepted as a degree-seeking candidate in the Graduate School of Engineering and Management in January 2004. Following graduation, he will be assigned to the 4th Space Operations Squadron, Schriever AFB, Colorado Springs, Colorado.

REPORT DOCUMENTATION PAGE

Form Approved
OMB No. 074-0188

1. REPORT DATE *(DD-MM-YYYY)*	**2. REPORT TYPE**	**3. DATES COVERED** *(From – To)*
21-03-2005	**Master's Thesis**	Jul 2004 – Mar 2005

4. TITLE AND SUBTITLE

Structures of Angled Aerated-Liquid Jets in Mach 1.94 Supersonic Crossflow

5a. CONTRACT NUMBER

5b. GRANT NUMBER

5c. PROGRAM ELEMENT NUMBER

6. AUTHOR(S)

Dixon, Dion, R., 1st Lieutenant, USAF

5d. PROJECT NUMBER

5e. TASK NUMBER

5f. WORK UNIT NUMBER

7. PERFORMING ORGANIZATION NAMES(S) AND ADDRESS(S)
Air Force Institute of Technology
Graduate School of Engineering and Management (AFIT/EN)
2950 Hobson Way
WPAFB OH 45433-7765

8. PERFORMING ORGANIZATION REPORT NUMBER

AFIT/GAE/ENY/05-M07

9. SPONSORING/MONITORING AGENCY NAME(S) AND ADDRESS(ES)
N/A

10. SPONSOR/MONITOR'S ACRONYM(S)

11. SPONSOR/MONITOR'S REPORT NUMBER(S)

12. DISTRIBUTION/AVAILABILITY STATEMENT
APPROVED FOR PUBLIC RELEASE; DISTRIBUTION UNLIMITED.

13. SUPPLEMENTARY NOTES

14. ABSTRACT

The structures of aerated-liquid jets injected into a supersonic crossflow have been studied experimentally. Aerated-liquid injectors with diameters of 0.020", 0.040" and 0.060" were flush mounted on the bottom plate of a supersonic wind tunnel to provide normal and angled injection. Freestream Mach number and temperature were held constant at 1.94 and 500 °F, respectively. Water at room temperature was used as the liquid injectant and nitrogen gas used as the aerating gas. Wide ranges of test conditions for injection angle (θ), injector orifice diameter (d_0), jet-to-air momentum flux ratios (q_0), and gas-to-liquid ratios (GLR), were studied. Injection angles were varied from 45° downstream to 90° (normal to freestream). Jet-to-air momentum flux was varied from 1% to 15% of the freestream and gas-to-liquid ratios from 0% (pure-liquid injection) to 10%. Shadowgraph and laser sheet illumination techniques were used for spray visualization while a phase Doppler particle analyzer (PDPA) was utilized to quantitatively measure droplet and spray plume properties. The data from all three methods were used to develop correlations for the droplet and spray plume properties for aerated-liquid jets using a linear fit of the base-10 logarithm coefficients. Correlations relating penetration height and spray plume width of the injected spray to the above listed parameters, as well as the normalized axial distance downstream of the injector, x/d_0, were formulated based on all three measurement techniques. Results indicate that a reasonable prediction of penetration height, spray plume cross sectional area, and local equivalence ratio can be obtained from PDPA data, while other visualization techniques tend to under-predict such quantities.

15. SUBJECT TERMS
Scramjet, aerated-liquid injection, supersonic combustion, supersonic crossflow

16. SECURITY CLASSIFICATION OF:			**17. LIMITATION OF ABSTRACT**	**18. NUMBER OF PAGES**	**19a. NAME OF RESPONSIBLE PERSON**
REPORT	**ABSTRACT**	**c. THIS PAGE**			Ralph A. Anthenien, PhD (ENY)
U	**U**	**U**	**UU**	82	**19b. TELEPHONE NUMBER** *(Include area code)* (937) 255-3636, ext 4643; e-mail: Ralph.Anthenien@afit.edu

Standard Form 298 (Rev: 8-98)
Prescribed by ANSI Std. Z39-18